National University of Lesotho

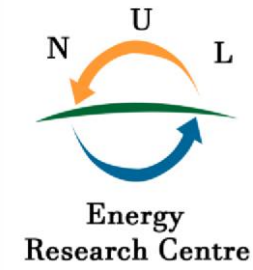

Design of a standalone hybrid solar-wind system with pumped hydro storage along Likhaebaneng river in Quthing district, Lesotho

Khiba Pitso (202202549)

A dissertation submitted in partial fulfilment of
the requirements for the degree of

Master of Science in Sustainable Energy

Offered by the

Energy Research Centre
Faculty of Science & Technology

June 2024

Abstract

Extending the power grid to all villages in Lesotho, a country characterized by rugged terrain comprising mountains and hills, is nearly financially unfeasible. Consequently, the nation suffers from escalating poverty due to insufficient access to electrical energy. The most viable and sustainable solution to provide electricity to unelectrified areas is to harness the renewable resources abundant in such regions. However, many renewable energy technologies face intermittency issues because they rely on natural resources with diurnal and seasonal patterns for power generation. Thus, it is necessary to consider complementary energy storage systems. The pumped hydropower plant emerges as a viable option for hybrid systems seeking efficient energy storage solutions. The present study examines the planning of a pumped hydroelectric power station situated in the Quthing district, Lesotho, utilizing the resources of the Likhaebaneng River, and the solar radiation and wind resources available in the area. The research site is positioned at Latitude -30.352244 and Longitude 28.160639, while the river under consideration boasts an average flow rate of 0.3 cubic meters per second and a gross head of 301 meters. The pumps, powered by both solar and wind power, are employed to pump water from the lower reservoir to the upper reservoir via a succession of 14 cascaded reservoirs. The turbine utilized for this generation process is the 5 kW Turgo turbine.

In the study area, the average scaled annual solar insolation and wind speeds are measured at 5.19 kWh/m²/day and 4.85 m/s at 30 m above ground level (a.g.l), respectively. The hybrid optimization model for electric renewables (HOMER) software was employed to model, simulate, and optimize the hybrid system consisting of solar, wind, and hydropower. The chosen optimized system in this study, featuring a maximum wind power output of 3,000 kW and a maximum PV power output of 4,568 kW, demonstrated a Net Present Cost (NPC) of $46.48 million and a levelized cost of energy (LCOE) of $0.2053 per kWh, which is equivalent to M3.80 per kWh. The system annually generates 8,074,658 kWh from solar resources, constituting 58.2% of the total production. Additionally, 5,797,867 kWh per year is generated from wind resources, accounting for 41.8% of the solar / wind system's total annual energy production of 13,872,525 kWh while 2,228,537 kWh is generated from PHES annually with the efficiency of 84.15 %. The consumption amounts to 8,764,589 kWh per year, resulting in an excess energy production of 28.9%.

Acknowledgements

First and foremost, I want to express my deepest gratitude to my Lord and Savior Jesus Christ for providing me with wisdom, strength, courage, and financial support throughout this journey.

I would like to extend my heartfelt thanks to my supervisors, Dr. Khaba and Dr. Makhele. Your tireless support from the beginning until now has made my work incredibly easy. I am truly grateful for your guidance and encouragement.

To the entire ERC team, I am not sure if you are aware of the tremendous change you have brought to our country. You are champions, and I appreciate your dedication and hard work.

To my two beautiful daughters, this is for you. Your presence has been a constant source of inspiration and motivation.

Lastly, my special thanks to my beautiful wife. God was truly thinking of me when He made you. Thank you for everything; we literally wrote this paper together. Your love, support, and encouragement have been invaluable.

Thank you all for your support and encouragement.

Contents

List of Figures

List of tables

1. Introduction

To fulfil their commitments within the framework of the Paris Agreement, numerous governments are enacting measures aimed at promoting the expansion of renewable energy sources [1] [2]. The increase in the adoption of renewable energy sources is primarily propelled by wind and solar power, which together make up approximately 90% of renewable energy capacity (excluding hydropower) [1], [3]. As a nation, Lesotho bears a moral responsibility to actively contribute to the realization of the Paris Agreement. This international accord, among its numerous objectives, strives to empower countries to prevent the global average temperature from exceeding a 2-degree Celsius increase. By participating in this effort, Lesotho stands to gain the numerous advantages associated with a global shift towards clean and sustainable development [4].

1.1 Background

Electricity is undoubtedly one of the major needs for modern society and plays a pivotal role in the economic growth [5]. On the other hand, if the current global energy policy remains unchanged, the International Energy Agency forecasts a 70 % increase in oil consumption and a 130 % increase in CO_2 emissions by 2050 [5]. This trajectory could lead to a substantial rise in the global average temperature, reaching 6 °C [5]. Several countries in West Africa are actively working towards reducing their greenhouse gas (GHG) emissions and have implemented policy targets to incorporate wind, solar, and hydropower into their energy mix to meet their energy demands. Table 1 provides an overview of the renewable energy policy targets set by these countries in West Africa. The majority of these countries are aiming to achieve their targets by 2030, with the exception of Senegal and Burkina Faso. Senegal has set a goal of achieving at least 15 % energy independence by 2025, while Burkina Faso has set a more ambitious target of 50 % renewable energy in its energy mix by 2025.

Table 1 Overview of policy targets for renewables for West African countries [6]

Country	Energy policy targets for solar/wind/hydro
Niger	250 MW RE by 2030, of which 130 MW hydro and 20 MW wind
Mali	More than 100 MW of renewable power capacity installed by 2020, mainly solar, wind, small hydro and biomass, to attain a 10% share of RE in the electricity mix
Nigeria	Ensure 10% of hydro in power production by 2030 and 6% of solar; no quantified wind power target, but "developing wind energy as an alternative renewable energy resource" to "integrate this with other energy resources into a balanced energy and electricity mix" is mentioned as key objective.
Gambia	44 MW hydro, 50 MW solar, 20 MW wind installed capacity by 2030
Guiné-Bissau	72 MW of RE capacity installed by 2030, of which 53 MW hydro, 15 MW solar and 2 MW wind power
Guinée-Conakry	30% of electricity production from renewable sources by 2030 (excl. biomass); 50 MW installed capacity of wind and solar and 1650 MW of hydropower
Ghana	RE penetration of 10% by 2030, with 150-250 MW utility-scale solar power, 50-150 MW utility-scale wind power, 150-300 MW small/medium hydropower
Togo	67.5 MW of solar, 24 MW of wind, 115 MW of medium/large hydro, and 70 MW of small hydropower capacity by 2030
Senegal	Achieve rate of energy independence of at least 15% by 2025 from using renewable sources (without biomass); solar, wind and hydropower all mentioned as candidates
Burkina Faso	50% of RE in "energy mix" by 2025; wind energy potential "worthwhile to evaluate"

The Kingdom of Lesotho has recently adopted the National Climate Change Policy, a strategic framework spanning from 2017 to 2027 [7]. This policy aims to address the pressing issue of climate change by incorporating various policy statements, including focusing on advancing renewable energy sources [7]. Studies indicate that Lesotho has an abundance of untapped renewable energy (RE) resources such as wind, solar, and hydropower which can be very useful in the generation of clean energy, especially for remote and inaccessible areas like the highlands and specific regions such as Thaba-Tseka, Qacha's Nek, Mokhotlong, and Quthing districts. According to Tsoeu-Ntokoane *et.al.*, wind potential exceeds 1,000 W/m^2/day in certain areas of the country, and global horizontal irradiation exceeds 5.3 kWh/m^2/day in most parts of the country [8], while Taele *et.al.* claim that pumped storage systems have well over 3000 MW viable potential in Lesotho [9].

Currently, when it comes to utility-scale energy storage systems, pumped hydroelectric storage (PHES) stands out as the most economically efficient technology for the storage of significant quantities of electrical energy [10]. In PHES systems, electricity is generated by a hydro turbine when there is high demand for energy. This is made possible by utilizing water that has been previously pumped and stored in an upper reservoir. The performance and efficiency of these systems are influenced by factors such as pressure losses, the characteristics of the pump and

turbine, electrical losses, and losses specific to the plant that are dependent on the gross head (the vertical distance between the upper and lower reservoirs) [11].

The intermittent nature of Renewable Energy Sources (RES) needs to be taken into consideration when designing a PHES. Hydropower generation possesses several distinct advantages, including quick start-up, great flexibility, and exceptional regulation capacity. These qualities make it well-suited for complementing the generation of wind and photovoltaic (PV) power [12]. Ma et al. provided evidence of the technological viability of an independent wind-PV hybrid system incorporating a pumped storage power station for a secluded island located in Hong Kong [13]. China is in the process of constructing a series of Hydro-WindSolar Clean Energy Bases (HWSCEBs) through the integration of large-scale RES with existing hydropower stations [14], [15]. This approach aims to facilitate the widespread incorporation of new renewable energy on a significant scale [15], [16]. Figure 1 shows the schematic diagram of cascade hydropower stations along with the pumping station for pumping water from the lower reservoir to the upper reservoir and the solar and wind farms, to provide electrical power required for pumping the water.

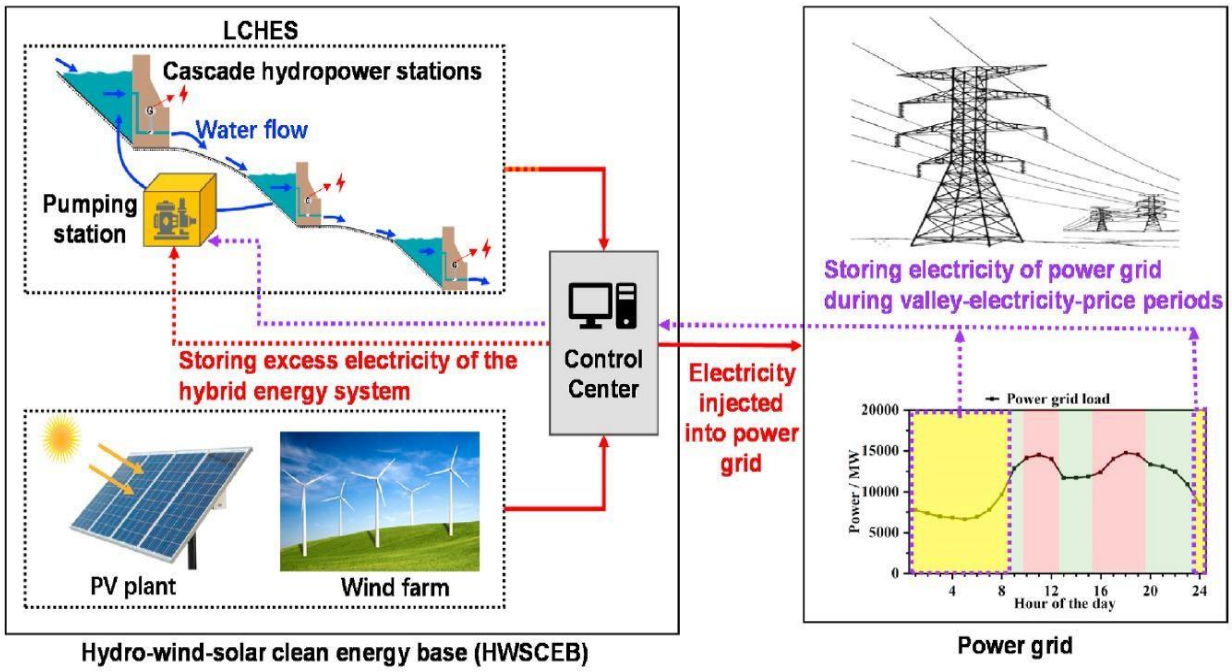

Figure 1 Schematic diagram of the large-scale cascade hydropower energy storage system (LCHES) [14].

Looking at the hydropower potential that pumped storage systems have, along with the wind and solar potential in the study area, the hybrid solar-wind with cascaded pumped hydroelectric storage (PHES) can be used to generate electricity for rural communities in the district. The proposed site for the PHES in Quthing is shown in Figure 2. The proposed solution is already in use in other parts of the globe. Previous research efforts have primarily concentrated on investigating the synergy between two specific energy systems, such as wind-hydropower, wind-photovoltaic (PV), and PV-hydropower hybrid systems [12]. These studies have explored the complementary relationship and potential benefits derived from combining these energy sources [12]. Ma et al. [13] have successfully showcased the technical viability of an independent wind-PV hybrid system integrated with a pumped storage power station on a secluded island in Hong Kong. Furthermore, they conducted a techno-economic analysis to optimize the performance and cost-effectiveness of the standalone photovoltaic power generation system based on pumped storage [17].

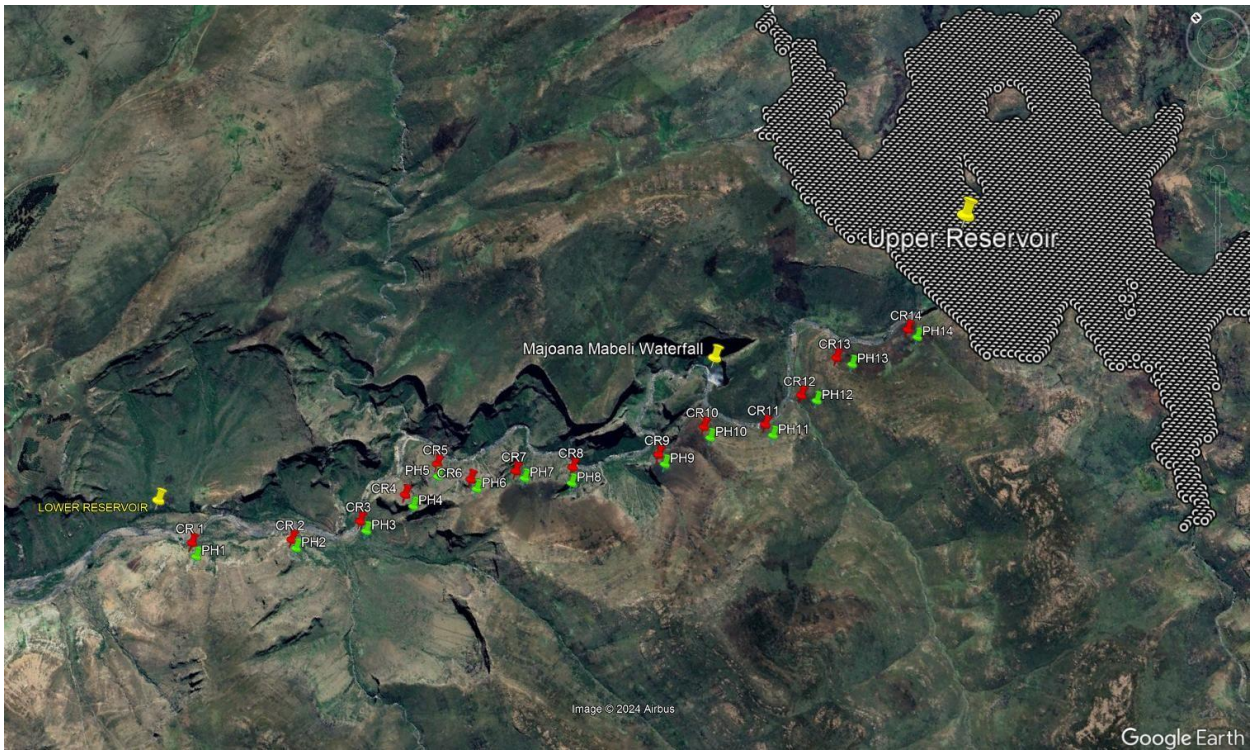

Figure 2 Proposed site for the cascade hydropower station

1.2 Problem Statement

Lesotho is predominantly characterized by its mountainous terrain, with elevations spanning from 1400 to over 3400 meters above sea level [7]. A significant portion of the population resides in rural areas, where everyday life can be challenging, and the lack of access to energy is one of the pressing issues affecting the local population [7]. Studies indicate that Lesotho has a hydropower potential of about 450 MW but only 72 MW has been harnessed so far [18]. This leaves remote and inaccessible areas like the highlands and specific regions such as the Thaba-Tseka, Qacha's Nek, Mokhotlong, and Quthing districts with very low electricity access [8]. The majority of the regions within the Quthing district are situated far away from the national power grid. Nevertheless, there exists an abundant supply potential of renewable energy resources such as water from the Quthing River and its tributary the Likhaebaneng River at upstream of the Majoana-Mabeli Waterfalls, wind, and solar energy that can be utilized to produce electricity and provide power to the local communities, thereby enhancing their quality of life. According to data obtained from the Lesotho Meteorological Services, the wind speed in the project area is 4.85 m/s at 30 m (a.g.l) while the daily irradiance is 232 W/m^2/day, with a good catchment area of 140 km^2 for the upper reservoir.

It is widely recognized that access to electricity directly contributes to economic growth. Although wind and solar resources are primarily intermittent in nature, there is a viable solution to address this challenge. By implementing pumped hydropower storage, the energy generated from solar and wind sources can be stored in the upper reservoir that can be built along the Likhaebaneng river and subsequently released as hydroelectric power during periods when there is insufficient sunlight or wind.

1.3 Objectives

The main objectives of this study revolve around the investigation of the design of a pumped hydroelectric storage (PHES) system using wind and solar resources available in the study area along with the sources of the Likhaebaneng river at upstream of the Majoana – Mabeli waterfalls near Lets'a – la – Letsie. The technical feasibility of integrating both wind and solar power in the design of a PHES system, the spatial and temporal variations of wind and solar resources at the location near the sources of the Quthing River, the environmental impact of

the proposed PHES system on the surrounding areas and the economic viability and costeffectiveness of implementing the system will also be assessed.

1.3.1 Assessing the potential for hydro, wind and solar power at the study area

The potential of a river to produce energy depends on various factors, including its flow rate, the catchment area supplying its water, and the local rainfall patterns. This study will consider these elements to make informed decisions for project implementation. Additionally, confirming the availability of adequate wind and solar resources is essential before proceeding, as these resources will power the solar pumps needed to transfer water from the lower to the upper reservoir. This step is among the initial actions required for the project.

1.3.2 Assessing feasibility of coupling wind and solar power for hydropower generation

Wind and solar energy sources are inherently intermittent, making it crucial to evaluate the potential of combining both energy sources for electricity generation in this study. In certain regions, these resources can complement one another; for example, when one resource is unavailable, the other may be accessible. This study will examine the extent to which these two energy sources can complement each other.

1.4 Research Questions

Specifically, the study aims to explore the following key research questions:

System Optimization: How can the operation and management of a pumped storage dam be optimized to efficiently accommodate intermittent wind and solar power generation, while ensuring optimal utilization of water resources and maximizing overall power generation capacity?

Energy Storage and Scheduling: What are the most effective strategies for storing excess wind and solar energy during periods of low demand and subsequently releasing it during peak demand periods, considering the specific characteristics of a pumped storage dam?

1.5 Justification

As previously mentioned in this study report, the availability of electricity has a significant impact on improving lives and boosting economies. Construction of a pumped storage system for hydropower generation in Quthing will bring substantial benefits to the local community. Due to the beauty of the surrounding Majoana-Mabeli Waterfalls and the Quthing River close

to the selected area, the project has the potential to attract tourists. Various businesses can be established, including the potential construction of world-class resorts in the region, resulting in increased revenue for local businesses and residents.

1.6 Dissertation Outline

The initial chapter of this study report serves as the project's introduction. Subsequently, the second chapter will delve into a review of relevant literature pertaining to the study. Chapter 3 will be dedicated to detailing the methodology used to address the research questions, while chapter 4 will focus on the presentation and discussion of the obtained results. Finally, the paper will conclude with chapter 5.

2. Literature Review

Given the rapid expansion of renewable energy systems, it is imperative to conduct thorough research on methods for storing the energy they generate. PHES stands out as one of the most efficient techniques for storing surplus energy during periods of low demand and releasing it during high-demand periods. These systems have the capacity to store substantial amounts of energy, which can significantly contribute to meeting a considerable portion of a country's energy requirements.

According to Zeidan et al., Morocco currently operates a PHES plant, which is the sole facility of its kind in the Middle East and North Africa (MENA) region, boasting a capacity of approximately 463 MW [19]. Furthermore, there is an ongoing pre-feasibility study for a 1000 MW pumped storage plant in Saudi Arabia [20]. This plant aims to provide power for 8 hours during peak load times, reducing the necessity for a 1000 MW thermal plant that consumes heavy fuel oil [19], [20].

2.1 Hydrology, water resources and hydropower potential

Hydrology is the scientific study of the effects, properties and distribution of water on the earth's surface in soil, underlying rock structures and in the earth's atmosphere. The notion of water resources is multifaceted and extends beyond its mere physical measurement, encompassing not only the 'flows and stocks' from a hydrological and hydrogeological perspective but also various qualitative, environmental, and socio-economic aspects. Hydropower potential is an amount of water flow which flows down a certain height. According to Peter H. Gleick, increasing levels of atmospheric concentrations of greenhouse gases in the atmosphere are causing alterations in climate, which have significant consequences on hydrology and its water resources [21]. Lesotho is certainly not exempt from the global challenge of climate change.

Before commencing with any water related project, a comprehensive study on the availability of resources in is important and It's important to mention that if a river intended for power generation lacks a gauging station, techniques for estimating the flow of ungauged catchments must be used to gather the essential data for the river involved in power generation.

2.1.1 Stream flow Statistics and Spatial Analysis Tools

This approach involves utilizing computer applications provided by the United States Geological Survey (USGS), namely StreamStats and BaSE [23]. StreamStats is a Geographic Information System (GIS) program that simplifies the process of acquiring stream flow statistics and drainage-basin characteristics for specific user-selected stream sites. Lekhanya [24] asserts that BaSE, on the other hand, can estimate the daily mean stream flow by comparing the stream flow percentile from a flow duration curve for a given day at an ungauged location, with the stream flow percentile from the flow duration curve for the same day at a reference stream gauge known to be hydrologically similar to the ungauged location.

To implement this method, it begins with delineating the ungauged stream using the delineation tool within StreamStats. Once the delineation process is finished, the software populates the basin characteristic statistics within StreamStats and allows users to download them as a Microsoft Database file. BaSE then matches this downloaded database with the closest gauged site's database file known to be hydrologically similar to the ungauged location. This reference gauged site shares similar local weather conditions with the ungauged location. The end result is an Excel report that contains data on stream flow, exceedance probabilities, basin characteristics, and hydrographs for the ungauged site. A potential issue with this approach is that the reference site might be located far from the ungauged site, which could result in the omission of localized summer thunderstorms [23].

2.1.2 Watershed area ratio method

This method is the most common that has been in use for decades in the estimation of ungauged catchments [23], [25]. The watershed area ratio method is primarily applicable for estimating flow in an ungauged catchment when a nearby gauged watershed serves as a reference. This method involves estimating the flow at an ungauged site by multiplying the measured flow at the nearby reference gauged watershed by the area ratio between the ungauged and gauged watersheds. Equation 2-1 can be used to estimate the flow at an ungaged location.

$$Q_{ungaged} = Q_{gaged} \times \frac{A_{ungaged}}{A_{gaged}} \qquad \textit{Equation 2-1}$$

Q and A in Equation 2-1 represent the flow rate of a river and the area of the watershed respectively. This method operates under the assumption that the flow rate scales directly with

the watershed area, implying that as the watershed area increases, the flow rate also increases at a constant rate per unit area. In essence, this assumption means that the flow per unit area remains consistent between the ungauged location and the gauged reference location [25].

2.1.3 Stream stage gauge

Given the topography of the study area, the most appropriate method for measuring flow rates is the stream stage gauge. According to Lekhanya, this method is currently employed by the Department of Water Affairs for the Quthing River [24], which means the same method can be employed in the flow estimations of the Likhaebaneng river since the two rivers are in the same location. This method is particularly well-suited for estimating flow rates in ungauged watersheds due to its simplicity and proven reliability over time [26].

2.1.4 Wind energy resources

Precise analysis of wind data plays a critical role in determining the potential amount of electricity that can be generated by wind in proposed locations [27]. In Africa, both the installed wind capacity and research efforts are, in general, quite limited [27]. Consequently, there is an urgent requirement to bolster both of these aspects, especially when considering that certain areas in Africa possess abundant wind resources, like the study area under consideration. According to Mpholo et.al., accurate wind data analysis is crucial in estimating the amount of potential electricity production in a proposed area [27]. The primary consideration when assessing a potential location for generating electricity using wind turbines is the wind speed. The Weibull function is the most commonly utilized and suggested distribution for characterizing wind speed in wind energy resource assessments [28]. Nevertheless, the Weibull distribution might not be suitable for representing wind patterns across various global terrains [29], in such cases the Rayleigh distribution function is utilised to determine the annual wind speeds. Rayleigh distribution is still identical to Weibull distribution function with a shape factor of 2 [30].

Mpholo et.al., state that the annual mean wind speed is just as important as the daily, monthly, and seasonal variations when assessing a location for wind energy production. Understanding both the overall energy potential over a specific period and the periodic fluctuations resulting from wind variability is essential for effective planning and utilization of wind resources [27].

Additionally, it's essential to be aware of the cut-in and cut-out speeds of the wind turbine as they play a crucial role in facilitating effective generation planning. Typically, the majority of wind turbines have a cut-in speed of 3 m/s, meaning they start generating electricity when the wind speed reaches this threshold. Conversely, there's a cut-out speed of 25 m/s, beyond which the turbine will cease operation as the wind speed is too high for safe functioning. Wind speeds below 3 m/s are also unsuitable for electricity generation as they are too low for the turbine to operate effectively. Understanding these speed parameters is vital for optimizing the performance and safety of wind turbines.

Another crucial factor to evaluate is the power density (PD), which represents the wind's intensity in the specific area per unit of space. PD is directly related to the potential power generation at the location and can be calculated using the following formula:

$$PD = 0.5\rho\overline{V^3} \qquad \text{Equation 2-2}$$

Where $\overline{V^3}$ is the mean wind speed cubed and ρ is the density of the surrounding air [27]. The density is estimated from pressure and temperature as:

$$P=P/RT \qquad \text{Equation 2-3}$$

where P is pressure in pascals and T is temperature in degree kelvin (K) and R is the dry air gas constant, calculated using the mean molar mass of 28.9645 g/mol [27], [31].

2.1.5 Solar energy resources

With the solar resources possessed by Lesotho in various areas around the country, the country is supposed to be injecting a lot of extra generated power in the Southern African Power Pool (SAPP) instead of purchasing electrical energy from Eskom and EDM. There are good solar resources in the study area that are sufficient to produce enough energy to pump water from the lower reservoir to the upper reservoir for the pumped hydropower storage. The research area's per-square-meter solar resource availability is depicted in Figure 38. Solar panels from the second generation are used to harvest these resources. The panels should be oriented at an angle that corresponds to the location's latitude for best performance. As the project is located in the southern hemisphere, proper alignment is also essential for optimizing the collection of solar resources; the panels must face north in order to maximize the harvest.

2.2 Renewable energy resources technologies

The worldwide electricity systems are swiftly shifting from fossil fuel-based power systems to renewable energy sources as shown in Figure 3. Approximately two-thirds of the annual net global capacity additions in power generation come from solar photovoltaics (PV) and wind, primarily due to the rapid decrease in the cost of PV and wind technologies [32].

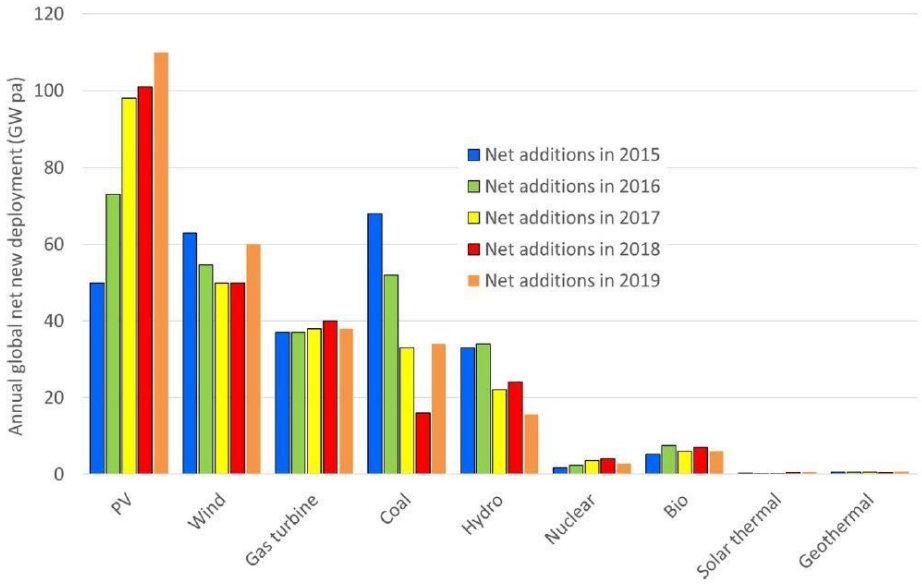

Figure 3 Net global annual generation nominal power capacity additions

2.2.1 Wind Technology

As the global need for electricity increases due to advancements in various aspects of life, it becomes essential for electricity generation to meet this rising demand. Employing clean and sustainable energy sources is pivotal in our efforts to reduce greenhouse gas (GHG) emissions as the electricity is being generated. Wind technology is one of the clean and sustainable energy generation techniques. The global expansion of wind energy for electricity production is rapidly gaining momentum [27].

An important first step in planning a wind energy project is estimating the amount of energy available in the wind at a proposed wind turbine site. The wind assessment approach is described by Wais [30], along with how it relates to the generation of electricity. When traveling at a constant speed v through the cross-sectional area A_R, the obtainable energy of the free-air stream is:

$$P_v = \frac{1}{2} \dot{m} v^2 = \frac{1}{2} \rho Q v^2 = \frac{1}{2} \rho A_R v^3 \qquad \text{Equation 2-4}$$

Where:

ρ = density of air

Q = volume flow passing through the given cross section A_R,

$A_R = \frac{\pi D^2}{4}$ = rotor cross-sectional area,

D = turbine rotor diameter v

= constant speed

Equation 2-4 shows how the wind rotor's area, air density, and wind speed affect the amount of power that is available in the wind stream [33]. The wind conditions at the proposed location of the wind turbine must be assessed, as even minor fluctuations in wind speed can significantly affect energy production. Given that wind speed varies, understanding the frequency distribution is essential. This provides information on the number of hours during which the wind velocity falls within a specific range [34].

2.2.2 Photovoltaic (PV) Technology

Photovoltaic (PV) technology stands as the leading method for harnessing solar energy, directly transforming it into direct current [15],[16]. PV power systems enjoy widespread use worldwide, with one of the most prevalent applications being PV water pumping systems (PVPS). These systems leverage solar energy to operate a solar pump, enabling the pumping of water for various purposes, such as drinking, irrigation, or, notably in the context of this study, the pumping of water from a lower reservoir to an upper reservoir for electricity generation. When designed effectively, these systems can offer significant cost savings and a good revenue generation when compared to grid-connected or diesel generator (DG) pumping systems for rural water supply. [15],[17],[18]. With the solar resources possessed by Lesotho

in various areas around the country, the country can actually generate more than enough energy to meet the demand and inject extra generated power in the Southern African Power Pool (SAPP) instead of purchasing electrical energy from Eskom and EDM.

The main purpose of a solar cell is to use the photovoltaic effect to convert light energy directly into electrical power [39]. When exposed to light energy from any source—natural or artificial—its electrical properties, such as resistance, voltage, or current, change. Solar modules are made up of solar cells [40].

2.2.2.1 Wafer-based Solar Technology (First generation)

In order to effectively make use of different absorption and charge separation techniques, solar cells are either composed of a single layer of light-absorbing material (single-junction) or use numerous physical configurations (multi-junctions). Crystalline silicon, including polycrystalline and monocrystalline silicon, makes up the first generation of wafer-based cells. To achieve the best possible light absorption, a thin layer of p-type material is built into the upper surface of the cell as depicted Figure 4. The p-type and n-type materials are surrounded by metal rings, which serve as the positive and negative output terminals, respectively [40] [41]. The semiconductor material serves as the PV cell's fundamental building block.

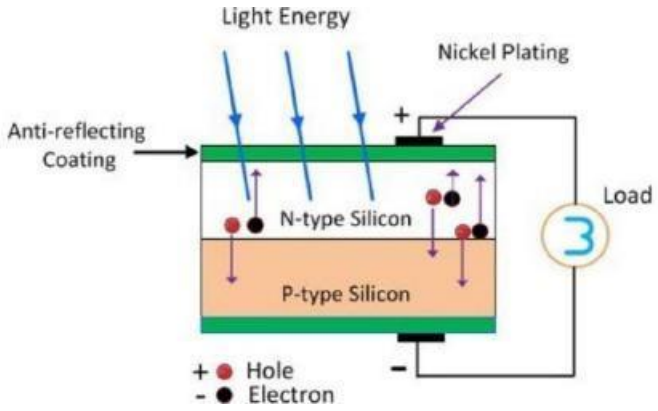

Figure 4 Wafer-based Solar Technology [41]

2.2.2.1.1 Monocrystalline Silicon Solar Cell

The Czochralski technique is used to create monocrystalline solar cells shown in Figure 5 from a single silicon (Si) crystal [39]. Usually, these Si crystals are made from massive, well-crafted ingots. A 16 % efficiency has been demonstrated using monocrystalline cells. Improved monocrystalline silicon solar cells now have an efficiency of 24.4 %, while enhanced multicrystalline silicon solar cells have reached a greater 19.8 % [39].

Figure 5 Monocrystalline Solar Panel [42]

2.2.2.1.2 Polycrystalline PV Modules

Polycrystalline PV modules in are made up of many crystals arranged in a single unit cell [39]. The production process is inexpensive, comprising the cooling of a graphite mold filled with molten silicon. As silicon solidifies, it creates crystals of various sizes, with flaws appearing at their borders. These flaws lower the modules' efficiency, which ranges from 18 % to 23 % in the laboratory and 14 % to 17 % in production [42].

Figure 6 Polycrystalline Solar Panel [42]

2.2.2.2 Thin Film Technology

These second-generation cells are composed of amorphous silicon, Cadmium Telluride (CdTe), and Copper Indium Gallium Di-Selenide. They are commercially accessible and widely employed in utility-scale solar power facilities due to their better performance in foggy environments [43].

2.2.2.2.1 Amorphous Silicon Solar Cell (A-Si)

Amorphous-Si modules are commonly utilized in pocket and desktop calculators, as well as solar panels for domestic and utility-scale power generation. These modules are made by depositing a thin film of silicon vapor (about 1 μm thick) onto a substrate material, such as

glass or metal. A transparent conducting oxide (TCO) is used in the setup to reduce series resistance by providing a lateral conducting channel for current, as shown in Figure 7.

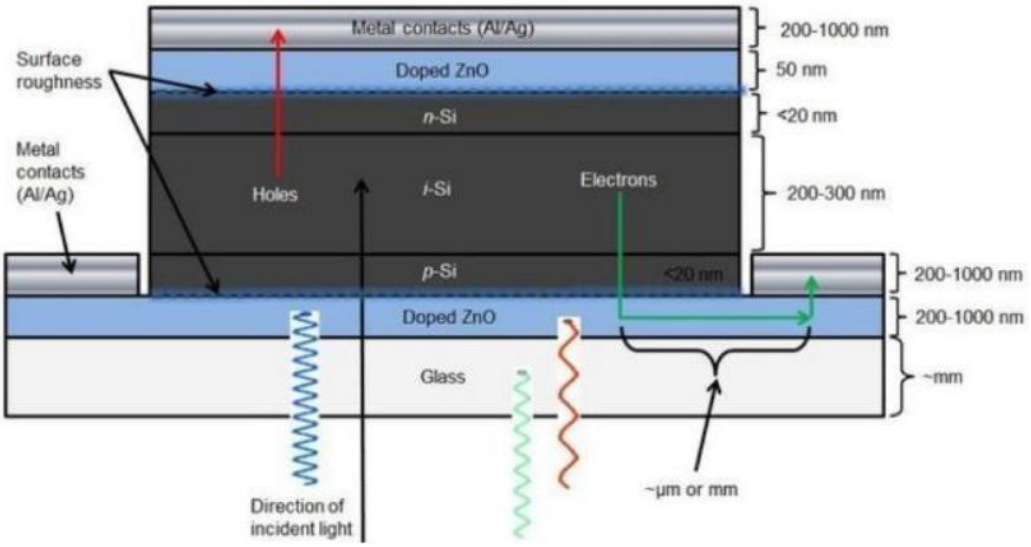

Figure 7 Amorphous Silicon Solar Cell Composition [44]

2.2.2.2.2 Cadmium Telluride (CdTe) Thin Film Solar Cell

Cadmium telluride (CdTe) photovoltaics consist of a thin semiconductor layer made from cadmium telluride, designed to capture and convert sunlight into energy (Figure 8) [44]. CdTe PV is the only thin-film technology that has lower costs compared to typical multi-kilowatt solar cells made from crystalline silicon. This technology has a few notable advantages, including lower life-cycle greenhouse gas and heavy metal emissions, a lower environmental impact, and quicker energy turnaround periods [45].

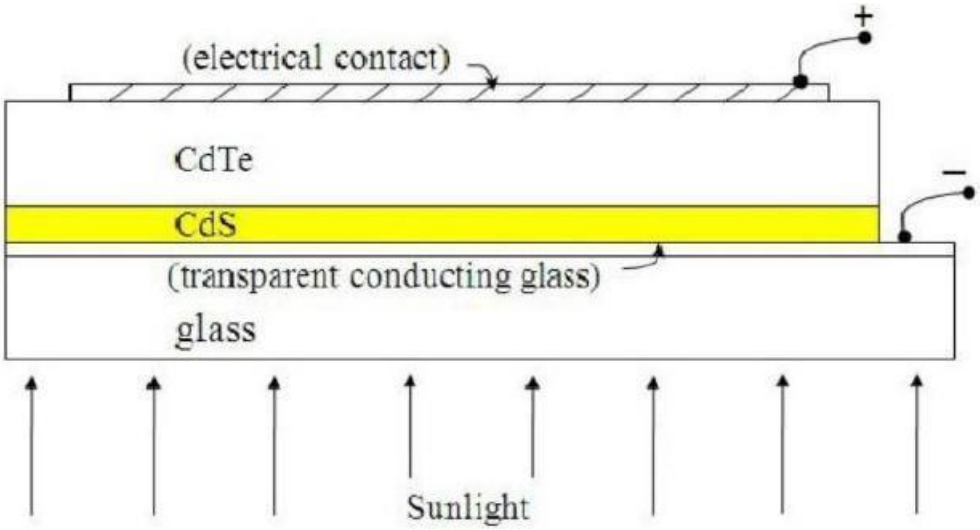

Figure 8 CdTe Thin Film Solar Cell Layers [44]

2.2.2.2.3 Copper Indium Gallium Di-Selenide (CIGS) Solar Cells

The cell's main components are the absorber CIGS and the buffer layer (CdS). Between these two layers is a thin layer identified as the ordered vacancy compound (OVC). The interface states between the buffer layer and the absorber give rise to this indeterminate layer, which is difficult to characterize exactly [46]. The buffer layer is covered with intrinsic (i-ZnO) and boron-doped (ZnO: B) layers. These layers, known collectively as transparent conductive oxide (TCO), are transparent to most of the solar spectrum due to their broad band-gap. The surface of the TCO layer is coated with an anti-reflection layer, MgF2, which enhances photon absorption [41]. According to Sarah and Roland, CIGS has a greater average efficiency than CdTe (about 10 % - 12 %), with some CIGS cells reaching up to 22.8 %. This enables CIGS to compete effectively with crystalline silicon (c-Si) wafer-based solar cells [41].

2.2.2.3 Third Generation Solar Technologies

The upcoming thin-film technologies are classified as third-generation solar technology. The majority of these are still in the early stages of development and research and are not yet accessible to customers [41]. Two of these technologies are Nano Crystal Based Solar Cells and Polymer Solar Cells (PSC).

2.2.2.3.1 Nano Crystal Based Solar Cells

Nanocrystal-based solar cells, also known as Quantum Dot (QD) solar cells [34], make use of nanocrystal-sized semiconductors, typically from transition metal groups. These semiconducting materials can attain efficiencies of up to 16.6 percent. QDs usually have a fundamental arrangement with layers of various chemicals placed on them. This design intends to increase efficiency by lowering the contact forces within the exciton and the nanoparticle surface [47].

2.2.2.3.2 Polymer Solar Cells (PSC)

A PSC is composed of thin functional layers that are serially connected and stacked up on top of a polymer foil. It functions primarily as a mix of donor (polymer) and acceptor. Various chemicals are used to extract sunlight energy, including organic components such as a conjugate/conducting polymer [47]. Figure 9 is a depiction of a typical organic bulk heterojunction device with layers of various materials, including a transparent bottom electrode of indium-tin oxide (ITO), a hole transport layer (HTL) similar to the donor polymer/acceptor molecule blend as the active layer, and a top electrode layer (usually metallic).

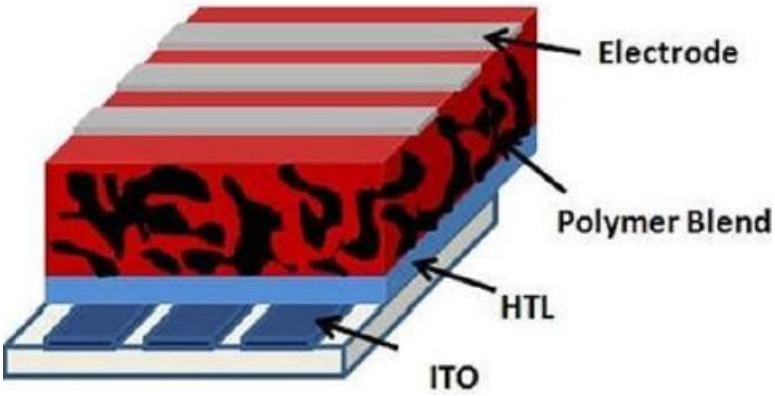

Figure 9 Polymer Solar Cells Layers [47].

2.2.3 Hydropower Technology

Hydropower station is the earliest and most mature renewable energy generation technology in the world. Moreover, until now the installed capacity is still increasing. Technically and financially, this energy source is recommended due to its fairly high efficiency, ranging from 75% to 85% throughout a wide range of flow [48]. Hydroelectric power holds significant value within an electricity system due to its ability to efficiently adapt to fluctuating electricity demands by adjusting water flow through the turbine. This reduces the reliance on slowerresponding coal-fired and nuclear power systems to track changes in electricity demand as it increases or decreases [49]. In pumped hydropower, water is stored in an upper reservoir and released during periods of high electricity demand. As the water flows through a turbine, it generates electrical power. The amount of power produced primarily depends on two key factors: the flow rate of the water and the head of the river, although other factors can also influence power generation.

2.2.4 Modelling pumped hydro storage as a battery in HOMER

Most renewable or low-carbon resources face a major challenge: their intermittent nature, which depends on ever-changing seasonal patterns. Wind and solar resources fall directly into this category. For example, in Lesotho, there is abundant wind during the winter months but very limited wind resources during the summer months. Conversely, solar resources are limited during the winter and abundant during the summer. To balance the intermittent nature of these resources, a more reliable renewable resource like water can be used. The pumped hydropower plant is a suitable alternative to consider as an energy storage device for hybrid systems.

HOMER is the industry standard software that is widely used to model and design renewable resources hybrid systems but it does not include an explicit component to model a pumped hydropower facility [50]. Nevertheless, a pumped hydroelectric storage can be modelled as a battery in HOMER.

Islam SM modelled a pumped hydro storage system as a battery in HOMER for a wind-dieselhydrogen hybrid system in Ramea, a small island in southern Newfoundland, Canada. In this model, the hydrogen energy storage system in HOMER was removed and replaced with a battery model. The overall efficiency of the battery was reduced to 70% to represent the typical efficiency of a pumped hydro energy storage system. HOMER sized the system by making energy balance calculations for each of the 8,760 hours in a year [51]. In this system HOMER suggested that the best battery bank should have 500 Trojan T – 105 batteries and based on the maximum power coming out of batteries, Islam SM selected a 250 kW converter for the system. The simulated electrical performance of the hybrid energy system is shown in Figure 10.

Figure 10 Expected electrical performance for Ramea system [51]

According to Canales et al., there are challenges with Islam SM's approach to modelling pumped storage in HOMER. Canales et al. assert that for normal batteries, storage capacity depends on the rate at which energy is withdrawn. This is not the case for a hydropower plant, whose capacity is determined by the water balance and the size of its reservoir, making it less affected by the rate of energy withdrawal. Additionally, representing large hydropower plants with an enormous quantity of batteries can complicate the model, making it difficult to interpret the information and results, or to understand the implications in terms of equivalent units [52].

Canales et, al., suggest a slightly different approach to modelling pumped storage in HOMER. To represent a pumped hydropower system as an equivalent battery, the first step is to understand the characteristics of the pumped storage system [52]. These characteristics of the example used are listed in **Table 2**. With these characteristics known, canales et.al., claims that a pumped hydro storage can be modelled in HOMER.

Table 2 Main Characteristics of the pumped hydro storage used as an example

Characteristic	Symbol	Value	Units
Size of the reservoir	*Vol*	3600.00	m^3
Available head	*H*	10.873	m
Flow rate (turbines)	*Q*	0.10–0.50	m^3/s
Conversion efficiency	η	75%	…
Planning horizon	*Lifetime*	20	yr
Flow rate (pumps)	Q_P	0.2	m^3/s

Table 3 displays the relationship between a pumped storage and its equivalent battery. For example, pumped storage with the volume of 3600 m^3, 10.873 m head with the conversion efficiency of 75 %, if the flow rate (Q) is 0.3 m^3/s, the reservoir will be emptied in about 3.33 hours, the total energy (E_s) stored in the reservoir will be is 80 kWh and 24 kW of power. The equivalent battery capacity in Ah is 333.333 Ah with a charging current of 100 A [52].

***Table 3 Relationship between a pumped storage and its equivalent battery** [52].*

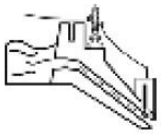	**Pumped hydro** *Vol:* 3600 m^3 *H:* 10.873 m η: 75%	Eq. (1) ≡ Eq. (2) Eq. (4) ≡ Eq. (6)			**Equivalent battery** Voltage: 240 V Round Trip Eff.: 100% Min. state of charge: 0
Q (m^3/s)	*Hours to empty*	E_S (kW h)	P (kW)	C_B (A·h)	I (A)
0.10	10.00	80.00	8.00	333.333	33.333
0.20	5.00	80.00	16.00	333.333	66.667
0.30	3.33	80.00	24.00	333.333	100.000
0.40	2.50	80.00	32.00	333.333	133.333
0.50	2.00	80.00	40.00	333.333	166.667

2.3 Defining a PHES

For over a century, PHES has played a vital role in facilitating load balancing within the electricity sector. The PHES process involves transferring water from a lower reservoir to a neighbouring upper reservoir during periods of excess power generation such as windy and sunny days. Subsequently, the stored water is released back to the lower reservoir via a turbine to generate electricity during times of insufficient supply such as in the evening. According to Blakers et.al, PHES makes up approximately 96% of the world's storage power capacity and accounts for about 99% of the global storage energy volume. Several countries have significant PHES capacity at their disposal, which plays a crucial role in balancing the supply and demand of electricity [49]. Figure 11 displays the substantial PHES capacities for some countries. Japan has the highest PHES power capacity followed by Taiwan, while India has the lowest of all the listed countries.

PHES stands out as an energy storage system (ESS) known for its extended lifespan, adaptability, and cost-effectiveness in terms of maintenance [53]. The energy stored in a PHES system relies on the interplay between photovoltaic (PV) and wind generation and energy demand [54], where the generated power (PGen) must align with the power required to meet the load demand (PDem). These relationships are represented by Equation 2-5 and Equation 2-6 respectively.

$$P_{Gen}(t) = P_{PV}(t) + P_{W}(t) \qquad \textit{Equation 2-5}$$

$$P_{Dem}(t) = P_{Gen}(t) +/- P_{PHES}(t) \qquad \textit{Equation 2-6}$$

Where $P_{PV(t)}$, $P_{W(t)}$, and $P_{PHES(t)}$ are power produced by solar plant, wind farm and PHES respectively. It should also be noted that

- If $P_{Dem}(t) > P_{PHES}(t)$, the extra power from the solar plant and the wind farm makes up the shortfall in the power generated from $P_{PHES}(t)$.

- If $P_{Dem}(t) = P_{PHES}(t)$, $P_{Gen}(t) = 0$; the power generated by $P_{PHES}(t)$ is just sufficient to supply the demand.
- If $P_{Dem}(t) < P_{PHES}(t)$, $P_{Gen}(t) < 0$; the excess power generated is stored by the P_{PHES}.

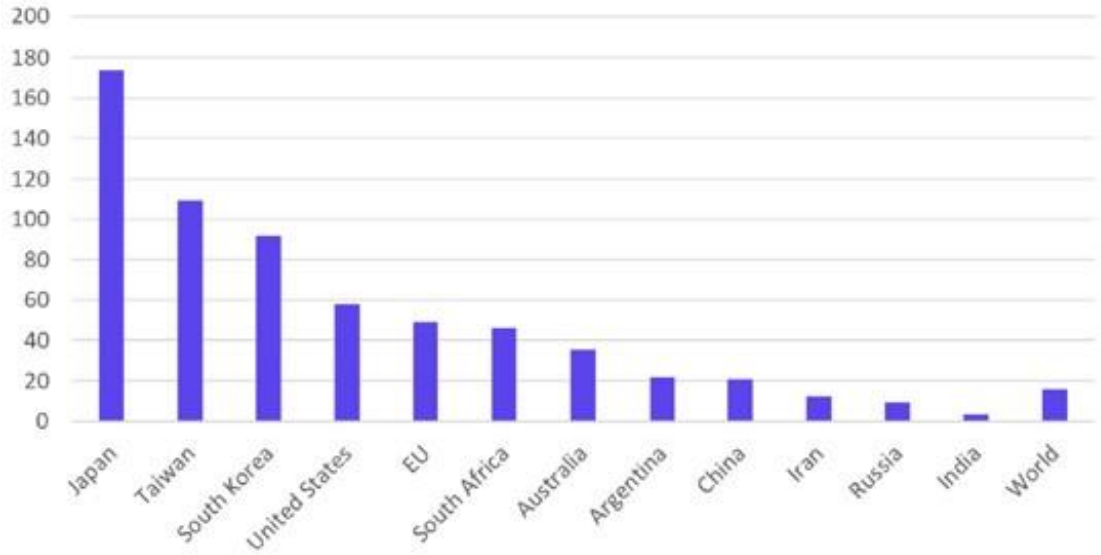

Figure 11 Pumped Hydro storage power capacity [49].

2.4 Storage system's components

The storage system comprises four main components: the upper reservoir, lower reservoir, powerhouse, and penstock.

Upper Reservoir

This is a water reservoir positioned at the upper location along the river, enabling an appropriate water level to facilitate the flow into the lower reservoir. The suggested upper reservoir site is depicted in Figure 2.

Lower Reservoir

This is a water storage pool located in a lower area in close proximity to the upper reservoir, positioned directly beneath it. The proposed lower reservoir is displayed in Figure 2.

Powerhouse

This is the location where electricity is generated using the water from the upper reservoir. The power station, or power house, houses all the necessary components for electricity generation,

including the turbine and generator, among others. The power plant will be positioned near the lower reservoir, in close proximity to the end of the water channel.

Penstock

This system comprises multiple interconnected pipes that link the upper reservoir to the lower reservoir. The length of the penstock is dependent among other factors on the size of the gross head and the amount of power to be generated. The PHES system components are displayed in Figure 12.

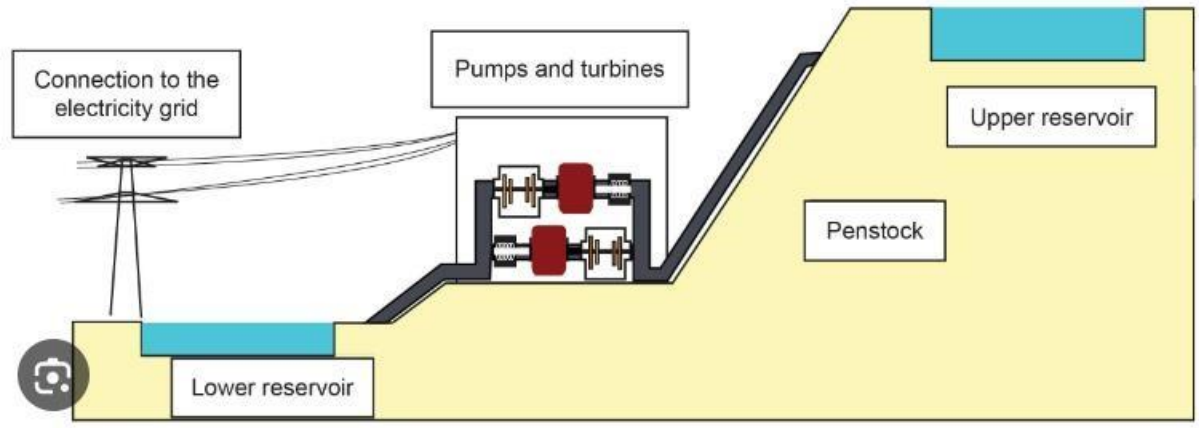

Figure 12 Storage System's Components

2.5 Pump / Turbine selection

Similar to hydropower, PHES facilities necessitate certain configurations, including a geodetic head (H) that represents the variation in water level between the upper and the lower reservoirs, and the potential for water utilization, determined by the usable flow rate (Q) [55]. The goal is to create designs and specifications that lead to the selection of a turbine or pump that provides the most cost-effective combination of the turbine itself, the associated water passages, and supporting structures [19].

The most cost-effective approach for pump or turbine selection is to opt for a pump that can also function as a turbine. Such pumps have the versatility to operate in two modes: as a turbine in generation mode (GM) and as a pump in pump mode (PM). The economic viability of a PHES system is significantly impacted by the selection of specific turbo machinery for the GM and PM. This choice can result in notable variations in both initial capital expenditures and operational efficiency [56].

Morabito et.al., points out that utilizing a centrifugal or diagonal pump as a turbine (PaT) in the GM represents a practical compromise between initial capital costs and performance [55]. In terms of maintenance, this approach offers several advantages when compared to custommade turbines. Pumps are relatively straightforward machines, easy to maintain, and are readily accessible in many developing nations [55]. From an economic perspective, it is frequently asserted that using Pumps as Turbines (PaTs) is a financially sound choice as it can result in capital payback periods of two years or less. This period is notably shorter than what is typically observed with conventional hydraulic turbines [55], [57]. However, it is important to note that the decision on turbine selection is not solely determined by these factors. Other considerations may override these factors in certain circumstances. For instance, in some systems, the geographical features and landscape may pose challenges that make choosing a particular type of turbine such as a PaT impractical.

2.6 Power potential of flowing water

Water is transformed into electricity through a series of energy conversions. According to Bernoulli's equation, which emphasizes energy conservation across different states, energy remains constant in various forms such as pressure, kinetic, or potential energy [58].

$$\frac{P_1}{\rho g} + \frac{V2_1^2}{g} + Z_1 = \frac{P_2}{\rho g} + \frac{V2_2^2}{g} + Z_2 \qquad \textit{Equation 2-7}$$

In the context of hydropower, the initial potential energy of water is converted into pressure energy, and subsequently into kinetic energy as the water passes through a turbine. The turbine facilitates the conversion of pressure and kinetic energy into mechanical energy. Finally, a generator transforms this mechanical energy into electrical energy, which is then made available for use by end consumers [58].

To determine the power potential of water in a river, it is essential to know two key factors: the flow of the river and the available head. The flow of the river refers to the volume of water, typically measured in cubic meters (m^3) or litres, passing through a specific cross-section of the river within a certain time frame [59]. Flow rates are commonly expressed in units like cubic meters per second (m^3/s) or litres per second (l/s). On the other hand, the head represents the vertical difference in elevation (measured in meters) through which the water descends.

The theoretical power (P) that can be harnessed from a given head of water is directly proportional to both the head (H) and the flow (Q).

2.7 Head assessment

There are a few methods that can be used to assess the head of the river that is intended to be used for the power generation. Three head assessment methods will be discussed in this section.

2.7.1 Altimeters

Altimeters prove valuable in feasibility studies for hydropower stations by aiding in the determination of elevation or high head [23]. Essentially, altimeters calculate altitude based on atmospheric pressure measurements. A pressure altimeter is essentially a barometer adjusted with a nonlinear scale to display altitude rather than pressure. Surveying altimeters typically exhibit errors within a 3 % range. Lekhanya asserts that this method can be rapid and effective, especially for medium and high elevations exceeding 40 meters [23]. However, it is important to note that since altitude is pressure-dependent in this approach; abrupt changes in atmospheric pressure can lead to readings differing by several meters, even when the actual elevation remains constant. In regions like Lesotho, where mountainous terrain can experience sudden temperature fluctuations affecting pressure, this method may not be the most convenient for conducting studies.

2.7.2 Direct Distance Measurement

Using a surveyor's transit on a tripod or a level fastened to a straight board, a contractor measures elevation using this method. For this process, a graded pole is also required. In addition, the measurements cannot be completed without the assistance of a second person. Using the transit level and the vertical measuring pole at particular areas of interest, a series of vertical measurements are taken as part of the measurement procedure. The aggregate of these individual height measurements yields the total height or elevation. This method's inaccuracy typically lies within 5 % on steep slopes, but it might vary between 10 % and 20 % on long, mild slopes. Even though this method is accurate, it is not recommended for use in rough mountainous terrain such as the area where the Likhaebaneng River is situated due to the challenges posed by multiple measurements in challenging topographical conditions.

2.7.3 Maps

Mapping is a great method; the main safety measure is to confirm that the study site is correctly identified. The quality and scale of the map determines how accurate the measurements are made using this method; higher elevations are better suited for it. Land surveyors can provide maps for a fee, but Digital Elevation Models (DEMs) can provide easily accessible maps. Because of these benefits over alternative approaches, using maps is the most appropriate way for determining elevation at the reconnaissance level in the research region.

3. Methodology

It is crucial to bear in mind that fulfilling the necessary geographical criteria for the site is a complex task. Hence, to reduce the overall expenses related to the project's capital infrastructure, it is imperative to explore and identify optimal locations that satisfy the most PHES installation needs [19].

This research comprises two concurrent phases (phase 1 and phase 2) that share a common abstraction point. The present investigation specifically addresses phase 1, while the other phase is the subject of a separate study. The delineation of catchment areas for the abstraction point and the region preceding the confluence of the two rivers will be accomplished through the Watershed Modelling System (WMS). This data will be utilized to compute the flow rates of the Likhaebaneng and Quthing rivers, which are the rivers involved in the study. To determine the ratios of water pumped from the lower reservoir to the upper reservoir by the two distinct systems, the flow rates of the two rivers will be assessed based on their respective catchment areas before the confluence of the two rivers. It is important to note that this study exclusively focuses on the Likhaebaneng River, excluding the Quthing River from its scope.

3.1 Study area

3.1.1 Location of the Likhaebaneng River catchment

The study area is located on the southern part of Lesotho in the Quthing district. The Likhaebaneng River catchment is located at upper Majoana-Mabeli waterfall (latitude -30.348225, longitude 28.164406) near the sources of Quthing River.

3.1.2 Topography and potential heads

Topography involves the examination of the Earth's terrain, which includes features such as mountains, valleys, rivers, and surface craters. Areas lacking natural land formations suitable for conventional high-head pumped hydro storage may not be feasible for this energy storage method. Additionally, topography plays a crucial role in determining the elevation of a river and the presence of energy resources in a given location. The designated site for the solar power facility in the study area benefits from favourable topography, ensuring prolonged exposure to sunlight throughout the day. This advantageous positioning allows for the continuous harvesting of solar energy, resulting in electricity production for extended periods. Likewise, the chosen location for the wind turbines is strategically situated in an area where wind

resources are most abundant, creating an exceptional opportunity for maximizing electricity generation. The topography of the study area is displayed in Figure 2. The methodology used to design a standalone hybrid solar-wind system with pumped hydro storage along the Likhaebaneng River in Quthing District, Lesotho, is illustrated in the flow chart shown in Figure 13.

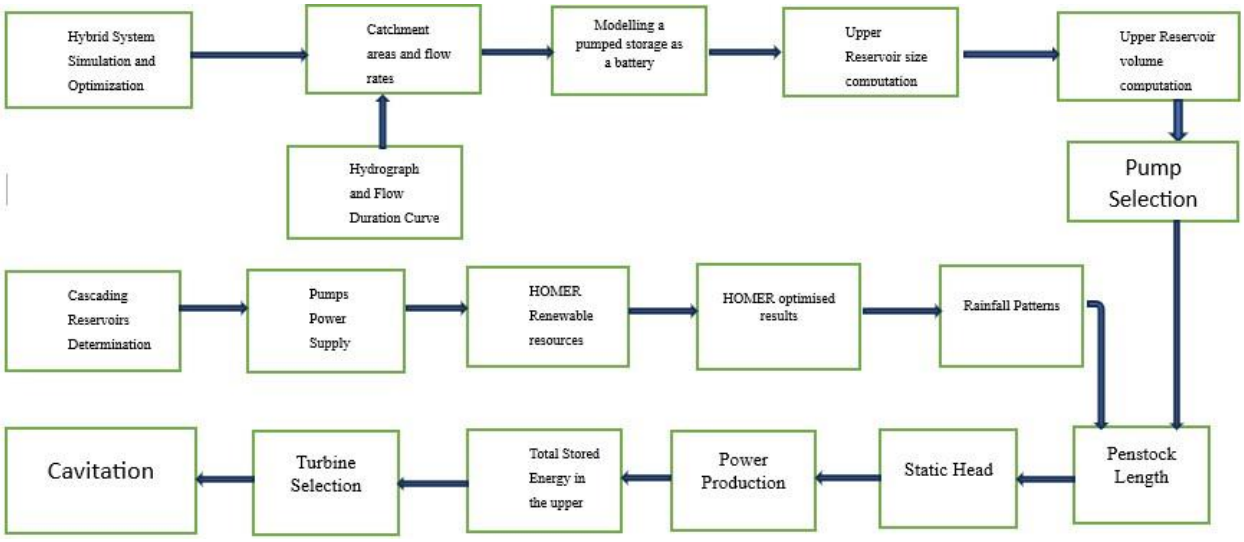

Figure 13 Methodology Flow Chart

3.2 The Hybrid System

The schematic of a hybrid system of wind and solar energy with cascaded pumped hydroelectric storage system is displayed in Figure 14. Wind, solar, and water are clean energy sources that, when effectively harnessed, can meet the growing energy demand, particularly in rural areas lacking grid extension but rich in these resources. High poverty levels and underdevelopment in many rural regions, especially in Sub-Saharan Africa (SSA), are often due to a lack of electrical energy. However, these areas possess abundant resources necessary for electricity generation, which can drive significant development and improve living standards. The system depicted in Figure 14 is among the most effective standalone solutions for supplying electricity in areas without grid extension or with unstable utility power. This study will utilize such a system to generate electricity in the study area. A cascade hydroelectric storage system will be designed, featuring multiple cascaded reservoirs, each with its own power source to minimize energy losses from long transmission lines. Water will be pumped from the lower reservoir to the upper reservoir through the series of cascaded reservoirs. It will then be released from the

upper reservoir through a turbine, generating electricity, which will be distributed to consumers via power lines.

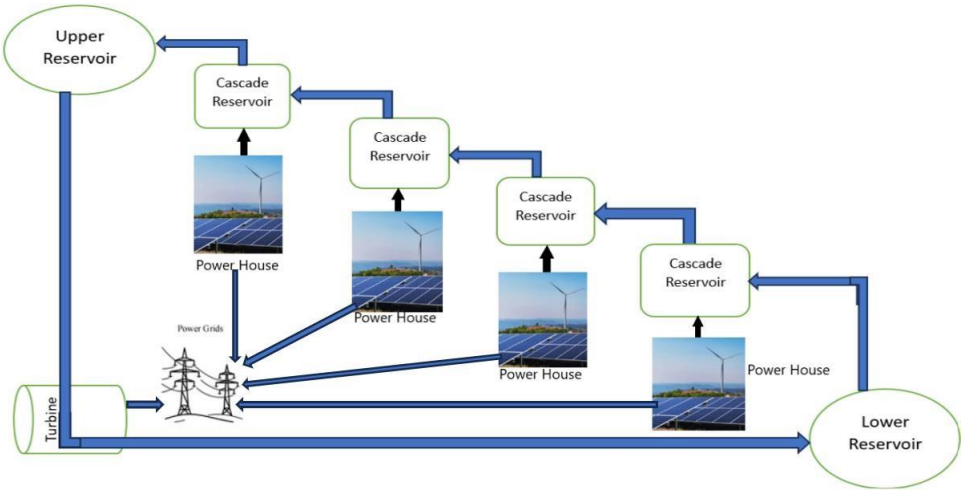

Figure 14 Schematic of a Hybrid wind and solar system with Cascade Pumped Hydroelectric Storage System

3.3 Hydrograph and Flow Duration Curve

A stream hydrograph plots the total flow carried in a stream against the amount of time that the stream flows while the cumulative frequency curve known as the Flow-Duration Curve (FDC) displays the percentage of time that the designated discharges were reached or exceeded within a given time frame. Numerous studies benefit from the flow-duration curve, particularly those that address reservoir sedimentation and water quality management [60]. Flow-Duration Curves (FDCs) are valuable tools for analysing catchment hydrological behaviour and streamflow characteristics. Their shape and slope provide insights into the variability of flow conditions at a site, as well as the catchment's flood-formation dynamics and low-flow characteristics [61]. The Likhaebaneng river hydrograph is depicted in Figure 15 and flow duration curve of the same river is displayed in Figure 16.

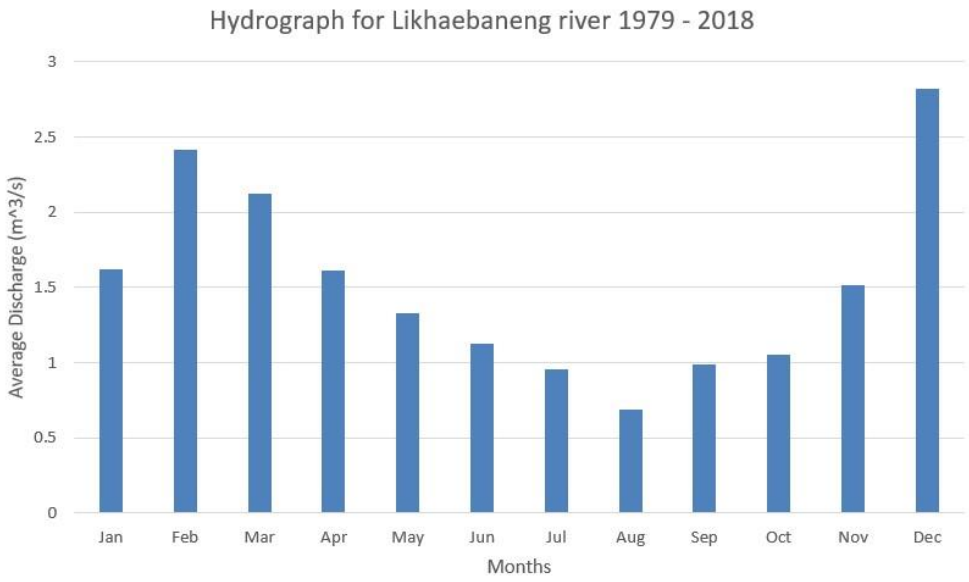

Figure 15 Likhaebaneng river Hydrograph

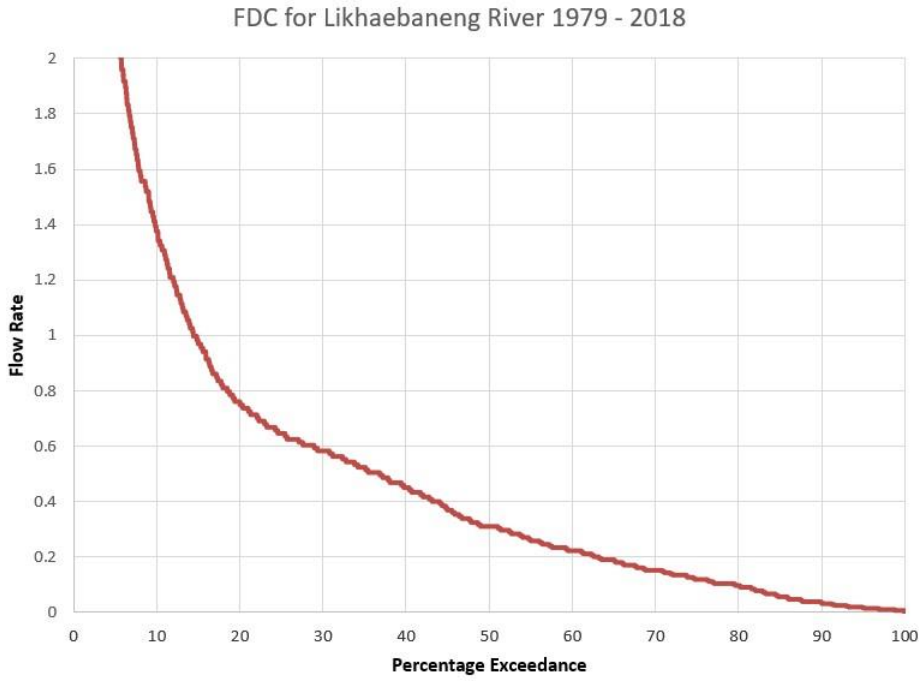

Figure 16 Flow Duration Curve for the Likhaebaneng river

3.4 Catchment areas, flow rates and design flow

The catchment areas were identified and delineated through the utilization of GIS and Watershed Modelling System (WMS) softwares. GIS is a Geographic Information System software that facilitates the visualization of geographic data, allowing users to create maps and necessary shapefiles for the task at hand. On the other hand, WMS is a proprietary software application designed for the development of computer simulations for watersheds.

The reservoirs' coordinates were extracted from Google Earth Pro. The shapefiles for the designated areas were generated using GIS and subsequently imported into WMS as GIS data. The digital elevation map (DEM) in Figure 17 is a depiction of the catchments of the entire country of Lesotho and all the catchment areas for the study are obviously located within this DEM.

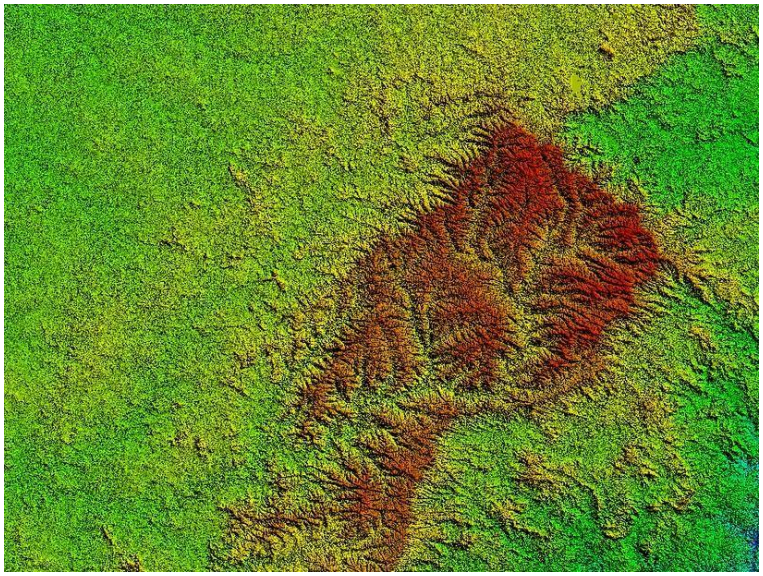

Figure 17 Digital Elevation Map for the entire country

Due to the absence of a gauging station on the Likhaebaneng River, the flow rate estimation will utilize the Watershed Area Ratio Method. This method involves determining the flow rate of the Likhaebaneng River by considering the catchment area of a nearby river equipped with a gaging station. In this study, the Quthing River at Hoko serves as the gauged reference. The process involves several sequential steps to ascertain the accurate flow rate of the Likhaebaneng River. Initially, the catchment area prior to the confluence of the two rivers (Quthing and Likhaebaneng rivers) will be computed, followed by the determination of the catchment area at the abstraction point. Subsequently, the catchment area of the Quthing River at Hoko will be calculated. Given that the Quthing River at Hoko has a gauging station and its flow rate is known, this information is then utilized to calculate the flow rate at the abstraction point by factoring in the corresponding catchment area. The resulting flow rate at the abstraction point, along with the calculated catchment area at that location, will then be used to determine the Likhaebaneng River's flow rate by factoring in the catchment area before the confluence. This established flow rate is crucial for determining the proportion of water to be pumped from the abstraction point to the upper reservoir through phase 1 system.

Design flow (Q_d) is the flow rate at which the plant generates its rated power. Studies recommend that the design flow should be between Q_{30} and Q_{70}. Opting for a lower flow rate (Q) result in underutilizing the river's capacity for power generation, meaning that a significant portion of the available water remains untapped. On the other hand, selecting a higher flow rate can lead to an inability to generate power for a substantial duration. The recommended decision for the design flow (Q_d) of the current study falls within the range of Q_{50} to Q_{60}, striking a balance that maximizes power generation without compromising operational efficiency for extended periods. As a result, Q_{50} will be used in this design to determine the design flow rate.

3.5 Modelling a pumped storage as battery in HOMER

A program called HOMER, or "Micropower Optimization Model," computes costs and energy balances for hybrid systems that are put together using pre-existing internal models. Systems including hydropower plants, solar panels, wind turbines, batteries, diesel engines, and other common parts of micro and small hybrid systems can be simulated with it [52]. HOMER, as useful as it is, has one key flaw: it lacks internal models for hydropower plants. This constraint is why a pumped storage system is frequently represented as a battery in software. The following section contains some fundamental terminology and equations to assist in the understanding of the links between a battery and a pumped hydropower storage.

According to Loucks and Van Beek, for hydropower generation, a cubic meter of water, weighing 10^3 kg, falling a distance of 1 meter, acquires 9810 j of kinetic energy. The energy generated in 1 second equals the watt of power (P) produced [62]. Hence an average flow (Q) in m^3/s falling a height (H) in meters and affected by an efficiency in conversion η, combining these variables in Equation 3-1 power in kilowatts can be obtained.

$$P = g \, x \, \eta \, x \, Q \, x \, h \qquad \textit{Equation 3-1 [50]}$$

By multiplying the power P by the duration of the time period t, one obtains the kilowatt-hours (kWh) of energy generated from an average flow rate of Q.

$$E = P \, x \, t \qquad \textit{Equation 3-2 [50]}$$

A battery's capacity (CB) is commonly measured in Ampere-hours. For example, a 100 Ah battery should be able to produce 100 A for one hour, 50 A for two hours, 25 A for four hours, 1 A for 100 hours, or any other combination that results in a 100 Ah product. In practice, this

is not always the case since, among other things, quicker discharge rates result in more energy loss due to internal resistance [50]. Hydropower generation on the other hand is not as heavily affected by its output and this is one of the two main reasons that justifies creating an equivalent battery for modelling a pumped hydro storage, instead of using one of the battery models found in HOMER software. Another strong point is that designing a battery allows users to set a high capacity and a specific voltage, which simplifies modelling the pumped hydro system with just one battery. Alternatively, different batteries can be used in the design phase to examine the impact of varying reservoir sizes. [50].

The total stored energy (E_s) of a battery can be determined using Equation 3-3

$$E_s = (V \times C_B) / 1000$$ *Equation 3-3 [50]* Similarly, the effective volume of the reservoir (in m^3) and the average power (kW) produced during the hours needed to empty the reservoir at an average flow rate (m^3/s) can be used to describe the total stored energy (kWh) in a hydropower plant, ignoring inflows and losses due to evaporation, withdrawal, or infiltration during the generation period. In order to do this, Equation 3-4 is applied.

$$E_S = (V \times P \times Q) / (Q \times 3600)$$ *Equation 3-4 [50]*

Using the data from

Table 4 and equations 3-1 to 3-4, the necessary values to model the pumped hydropower plant as a battery in HOMER for this study will be computed. The user needs to specify a few additional parameters when modelling a pumped storage as a battery. The minimum state of charge which is relative level of charge below which the battery bank is never brought is equal to zero. This suggests that the reservoir's effective volume may be completely exhausted for the purpose of producing hydropower. And lastly the battery voltage must also be selected [50]. The efficiency of the storage can be calculated through Equation 3-5.

$$\eta = \frac{Energy\ Out}{energy\ In} \times 100$$ *Equation 3-5*

Table 4 Main Characteristics of a Pumped Hydro storage

Characteristic	Symbol	Value	Units
Reservoir Size	Vol	176,960,504	m_3
Available Head	H	200	m
Flow Rate (Turbine)	Q	0.3	m^3/s
Conversion Efficiency	η	75	%
Planning Horizon	Lifetime	25	yr.
Flow rate (Pumps)	Q_P	0.14	m^3/s

3.6 Upper Reservoir size and volume computation

The size and volume of a reservoir are critical factors in designing a pumped hydroelectric storage system along with catchment area of the location where the reservoir is intended to be build. To determine the amount of electricity that can be generated, it is essential to know the reservoir's storage capacity. Equation 3-6 was used determine the volume of the upper reservoir. The reservoir location for the present study was identified along with all the tributary rivers around the Likhaebaneng River, which serve as water sources for the Likhaebaneng river. After identifying the location for the upper reservoir, the size and volume of were determined using Geographical Information System (GIS) technology. The detailed findings regarding the size and volume of the upper reservoir are discussed in the results and discussion section of this study.

Total reservoir volume = depth x length x width *Equation 3-6*

3.7 Pump Selection and Cascading Reservoir Determination

The comparison between two Lorentz pumps, namely the G200 – 244 and G125 - 404, led to the selection of the G200 – 244 for pumping water from a lower to an upper reservoir. This choice was primarily based on the G200 – 244 requiring fewer pumps when connected in both

series and parallel configurations. The specifications and pump chart for the G200 – 244 are presented in Figure 18 and Figure 19. Notably, the G200 – 244 has a maximum flow rate of 499 m^3/h equivalent to 0.14 m^3/s which is considered small in comparison to the design flow rate, while G125 – 404 has the maximum flow of 268 m^3/h which corresponds to 0.07 m^3/s. To boost the flow rate from 0.14 m^3/s to 0.3 m^3/s, the pumps must be connected in parallel. The determination of the number of pumps to be connected in parallel involves dividing the design flow rate by the maximum pump flow rate as indicated by Equation 3-7.

$$\text{Pumps in parallel} = \frac{\text{design flow rate}}{\text{maximum pump flow rate}} \qquad \text{Equation 3-7}$$

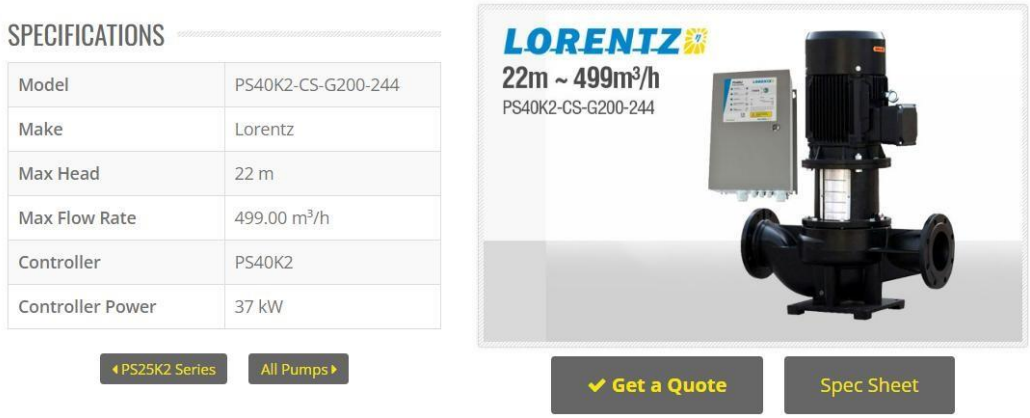

Figure 18 PS 40K2 - CS - G200 - 244 Solar water pump

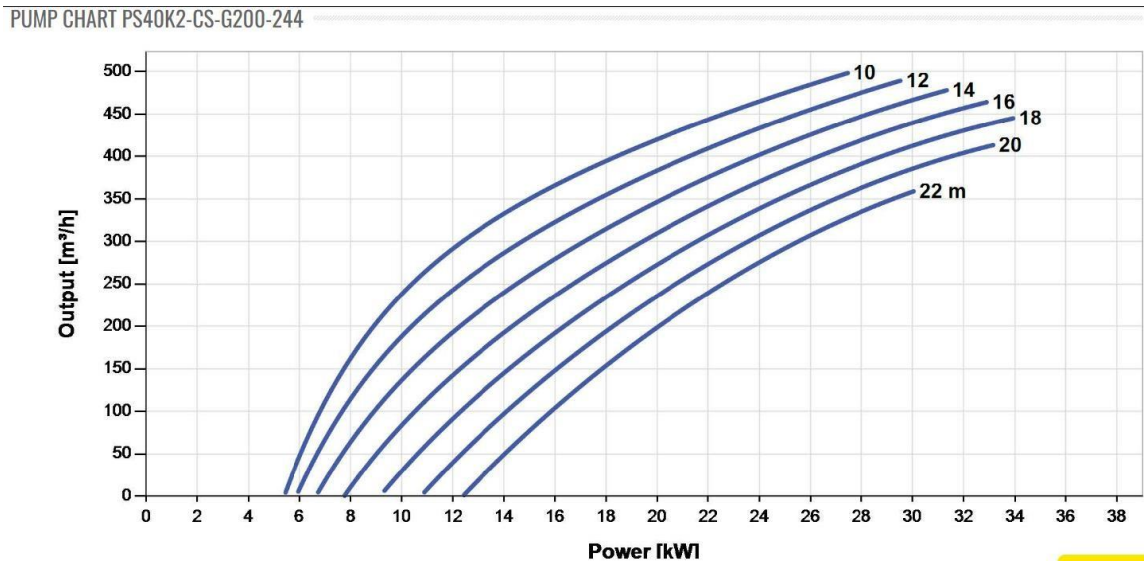

Figure 19 PS 40K2 - CS - G200 - 244 Pump Chart

Figure 20 PS 40K2 - CS - G125 - 404 Solar water pump

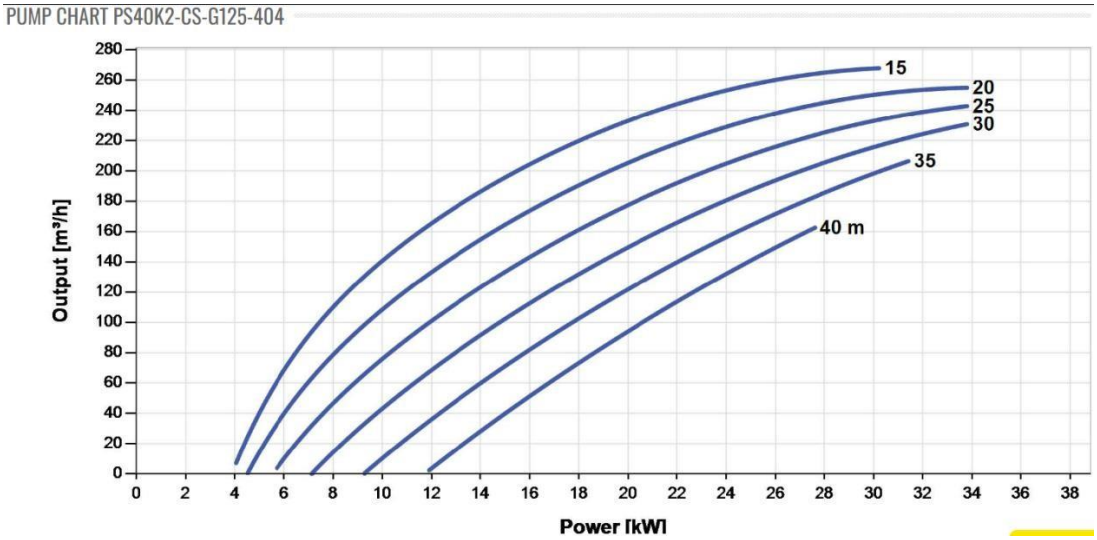

Figure 21 PS 40K2 - CS - G125 - 404 Pump Chart

As global energy supply issues and climate warming become more pressing, the transition to low-carbon energy on a global scale is urgently needed. In the current energy system, the robust development of new energy sources, such as wind and solar power, is crucial for promoting a low-carbon energy transition. However, the high fluctuation, randomness, and intermittency of wind and solar power make it challenging to meet real-time fluctuating power load demands and ensure the safe and reliable operation without the support of other flexible power sources [63].

One such flexible power source is PHES. This well-established and superior renewable energy source offers a broad regulation range, flexible operation, quick start-up and shutdown times,

and advanced technology [64]. It supplies the power system with a cross-seasonally controlled, long-term, large-capacity power source. The complimentary scheduling of hydro, wind, and photovoltaic (PV) energy can greatly alleviate the problems related to increased energy consumption by leveraging the vast cascade hydropower bases. The present study utilizes a cascaded reservoir system to facilitate the pumping of water from the lower reservoir to the upper reservoir. The number of cascading reservoirs is crucial to ensure that the design flow rate is maintained, despite the various factors involved in pumping and generation. The number of cascading reservoirs can be determined using Equation 3-8. The determination of the number of reservoirs also largely depends on the type and size of the pump. The types and the sizes of the pumps are displayed in Figure 18 and Figure 20.

Equation 3-8

$$\text{Number of cascading reservoirs } (N_{cr}) \text{ (G200 – 244)} = \frac{\text{Total head}}{\text{Pump head}}$$

3.8 Pumps Power Supply

Out of all the available RE sources, solar and wind are considered as the most abundant, developed, economically viable and commercially accepted [65]. In this study, the pumps responsible for transferring water from the lower to the upper reservoir will be powered by both wind and solar energy. To minimize significant power losses typically associated with lengthy power lines, each reservoir will have a dedicated small-scale solar and wind farm located next to it. The wind and solar plants will be designed using the Hybrid Optimization Model for Electric Renewables (HOMER). This is the industry standard for maximizing microgrid architecture across all industries including military bases, grid-connected campuses, and village power and island utilities. HOMER, a software application originally created at the National Renewable Energy Laboratory and later improved and provided by UL Solutions, combines three potent tools (optimization, simulation and sensitivity analysis) into one package to enable engineering and economics to function side by side [66].

HOMER is employed to facilitate the creation of diverse configurations for power plants. The tool incorporates various built-in elements such as photovoltaic (PV) panels, wind turbines, different types of utility loads, generators, converters, and battery backup, among others. Its primary function is to simulate different power plant schematics. These schematics are then

analysed to identify the most optimized power plant configuration based on factors such as operating cost, net present cost (NPC), gas emissions, and economic considerations [67].

3.9 HOMER Renewable resources and optimised system results

Today, hybrid systems have emerged as one of the most effective solutions for meeting the electrical energy needs of various regions. In practice, it has been proven that hybrid systems can be an appropriate solution, and by using a proper combination of the renewable resources, an affordable, clean, and reliable energy production system can be achieved [68]. HOMER is a trusted software known for its effectiveness in delivering reliable results for designed systems. In this study, it was used to assess the availability of renewable resources in the study area, with the results discussed and displayed in the results and discussion section. HOMER can design a hybrid system and provide the most optimal configuration. The optimized system for the present study is shown in Figure 41.

3.10 Rainfall Patterns

The majority of rainfall occurs during the summer months, while snow falls approximately eight times per year in the highlands and once every 2.3 years in the lowlands, predominantly during the colder months from April through September. [69]. This informs mainly the approach to use in the design of PHES in the study area. A clear picture of the rainfall patterns in the study area is depicted in Figure 46.

3.11 Penstock Length and diameter

The penstock length and diameter play a crucial part in both the pumping and generation period. The length of the penstock for the present study was measured using google earth pro. The diameter of the penstock was then calculated using Equation 3-9. This diameter value depends on the following factors:

1. The flow in the penstock
2. The inside walls of the penstock
3. The thickness of the walls of the penstock
4. The cost and installation of the penstock

Equation 3-9

$$D = \sqrt{\frac{4Q}{\pi v}}$$

3.12 Static Head

Static head consists of straight run head losses and friction losses. These losses are crucial to consider in the total static head. The straight run head loss is calculated using the Darcy Weisbach equation in Equation 3-10. Key factors in determining the static head include the length, diameter, and friction of the penstock, as well as the water velocity and the gravitational force acting on the water in the penstock. The Reynolds number is needed to determine the friction factor. The Reynolds number is calculated using Equation 3-11, and the friction factor is determined using Equation 3-12.

$$h_s = \frac{fLv^2}{2Dg} \qquad \textit{Equation 3-10}$$

$$R_e = \frac{v_x D}{\mu} \qquad \textit{Equation 3-11}$$

$$f = \frac{64}{Re} \qquad \textit{Equation 3-12}$$

Where h_s = straight run head losses

R_e = Reynold's number

$v_x = \upsilon$ = water velocity

μ = dynamic viscosity D = penstock diameter

Q = flow rate L = length of penstock g = gravity

3.13 Power Production

Fausto A. Canales and Alexandre Beluco explain that when one cubic meter of water with a mass of 103 kg descends by a meter, it gains 9810 joules (N·m) of kinetic energy, contributing to hydropower generation. The power produced in one second is equivalent to the watts of power P generated. Consequently, the average flow Q (m^3/s) descending a height h (m) and influenced by a conversion efficiency η power can be calculated using Equation 3-1.

To maximise the power production, the net head (h_n) is one of the critical components after determining the design flow. Net head is determined by considering the gross head (h_g) and friction losses (h_f) in a scheme, assuming that any local losses are negligible. The highest achievable power output can be calculated using Equation 3-13, given that the system's friction losses were previously assessed using Equation 3-20.

$$P = \rho \; x \; g \; x \; Qd \; x \; h_n \qquad \textit{Equation 3-13}$$

Where: ρ = density of water g = force of gravity

Q_d = design flow rate

Net head = Gross head – Head losses

$$h_n = h_g - h_f \qquad \textit{Equation 3-14}$$

Where h_f can be expressed as $h_f = cv^2$, with c being a constant. Substituting for h_f, the equation becomes:

$$h_n = h_g - cv^2 \qquad \textit{Equation 3-15}$$

The power (P) can be defined as:

$$P = \rho g h_n Q \qquad \textit{Equation 3-16}$$

Expressing $h_n = h_g - cv^2$ and Q = AV, the power equation becomes:

$$P = \rho g A V (h_g - cv^2) \qquad \textit{Equation 3-17}$$

The maximum power can be attained by differentiating P with respect to v and equating it to zero:

$$\rho g A (h_g - 3cv^2) = 0 \qquad \textit{Equation 3-18}$$

This simplifies to:

$$h_g = 3cv^2 \text{ or } h_g = 3h_f \qquad \textit{Equation 3-19}$$

This implies that for maximum power production, h_f can be calculated using Equation 3-20.

$$h_f = \frac{1}{3} h_g \qquad \textit{Equation 3-20}$$

The power capability of the generator, which constitutes to the output power, is derived using Equation 3-21

$$P_{av} = g \, x \, H \, x \, Q \, x \, \eta_t x \, \eta_g \qquad \textit{Equation 3-21}$$

3.14 Total Stored Energy in the upper reservoir

Likewise, neglecting any incoming or outgoing factors such as evaporation, extraction, or infiltration throughout the production phase, the overall stored energy (E) in a hydroelectric facility, measured in kilowatt-hours (kWh), can be explained by the effective reservoir volume (in cubic meters, m^3) and the mean power output (P) generated over the duration required to deplete the reservoir at an average flow rate (Q) in cubic meters per second (m^3/s) [70]. This relationship can be expressed using the following equation:

$$E = Vol \frac{}{(Q \, x \, 3600)} x \, P(Q) \qquad [70] \qquad \textit{Equation 3-22}$$

3.15 Turbine selection

Analysing another essential aspect for achieving maximum power generation involves directing attention to the turbine equipment. Selecting the appropriate turbine is critical in deciding whether the power plant can effectively produce the desired power capacity. The appropriate turbine model can be identified by consulting Figure 22. Once the appropriate turbine has been chosen, the subsequent stage involves establishing the turbine's specific speed and determining the diameter of the turbine runner.

In the current design, a 6-pole, 50 Hz generator is utilized and directly connected to the turbine. As a result, the specific speed of the Turgo turbine was calculated based on the rotational speed of the generator. The rotational speed was determined using Equation 3-23, while the turbine's

specific speed was obtained using Equation 3-24. According to Table 10 and Figure 22, the calculated specific speed and the net head, the appropriate turbine is Turgo turbine. The turbine runner is very crucial in the operation of the turbine.

$$N = \frac{60xf}{0.5\ x\ np}$$ *Equation 3-23*

$$N_s = \frac{N\ x\ \sqrt{Q}}{h_n^{0.75}}$$ *Equation 3-24*

$$D_{runner} = 84.5(0.79+1.602N_s)\frac{\sqrt{Q}}{N}$$ *Equation 3-25* Once the suitable turbine is chosen, the next crucial step is to identify the correct pumps that will transfer water from the lower reservoir to the upper reservoir where it will be released to the turbine for electricity generation.

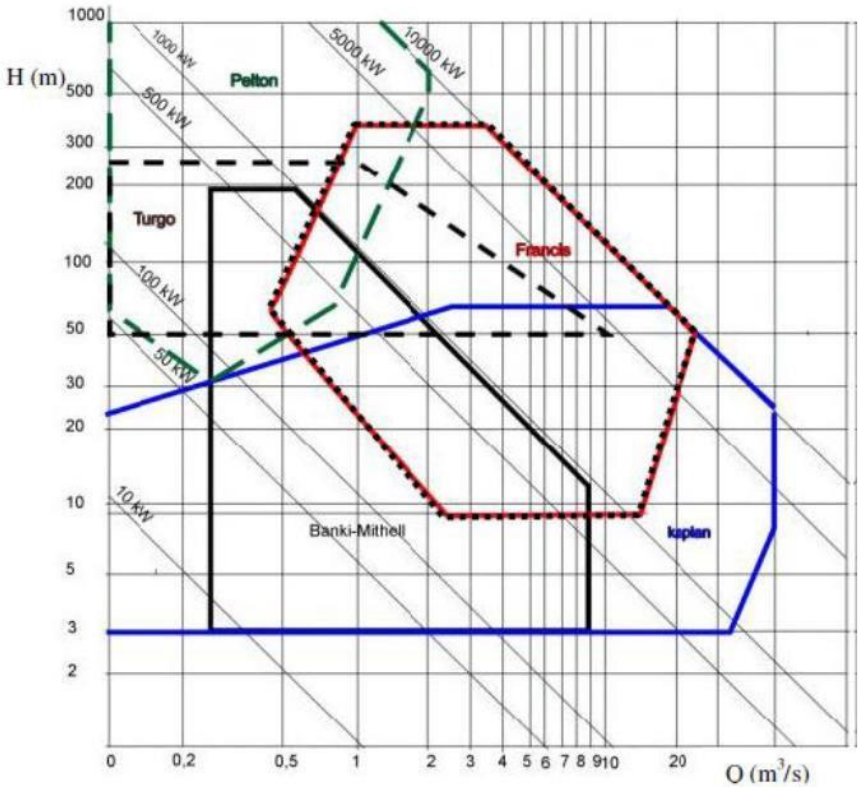

Figure 22 Operation areas of hydro turbines and their power

3.16 Cavitation

To prevent the formation of cavitation in the pumps, it is necessary to regulate the valve at the power house, thus ensuring a specific area for water flow and controlling the velocity at the valve outlet. It is crucial for the flow entering the penstock and exiting the valve to remain

consistent. Equation 3-26 - Equation 3-30 were utilized to determine both the cross-sectional area of flow and the velocity at the valve outlet. In Equation 3-9, the diameter (d) of the penstock was found to be 0.529 m; therefore the radius (r) of the penstock is calculated in Equation 3-26.

$$r = \frac{d}{2}$$ *Equation 3-26*

$$A_1 = \pi r^2$$ *Equation 3-27*

$$V_1 = \frac{Q_1}{A_1}$$ *Equation 3-28*

$$V_2 = \sqrt{Z_1 2g + \frac{1}{2g^{\cancel{1}}}\cancel{2g^{1}} + -Z_2 2g - Y_2 2}\quad \frac{V_2}{g}$$ *Equation 3-29*

$$A_2 = \frac{Q_2}{V_2}$$ *Equation 3-30*

Where:

A_1 = Area of penstock at the upper reservoir

A2 = is the cross-sectional area of flow at the exit valve

Q_1 = the design flow rate and it is the same as Q_2

Z_1 = the upper elevation at penstock inlet

Z_2 = the lower elevation at exit valve

Y_2 = difference between upper and lower elevations (head)

V_1 = velocity of water at the penstock inlet at the upper reservoir

V_2 = velocity of water at the exit valve

3.17 Environmental Impact Assessment

To comply with the Environmental Impact Assessment (EIA) requirements and preserve the natural aesthetics and continuity of the Majoana-Mabeli waterfall, it is crucial to prevent the mixing of water destined for the waterfall with the water utilized for power generation. To

achieve this, the suggested solution involves the installation of conduits. These conduits will transport water beneath the upper reservoir, ensuring a direct flow to the waterfall without commingling with the water pumped from the lower to the upper reservoir. The expected configuration of this installation, encompassing both the conduits and their outlet, is depicted in Figure 23; while Figure 24 depicts the upper reservoir surface extent with the conduits' installation configuration beneath.

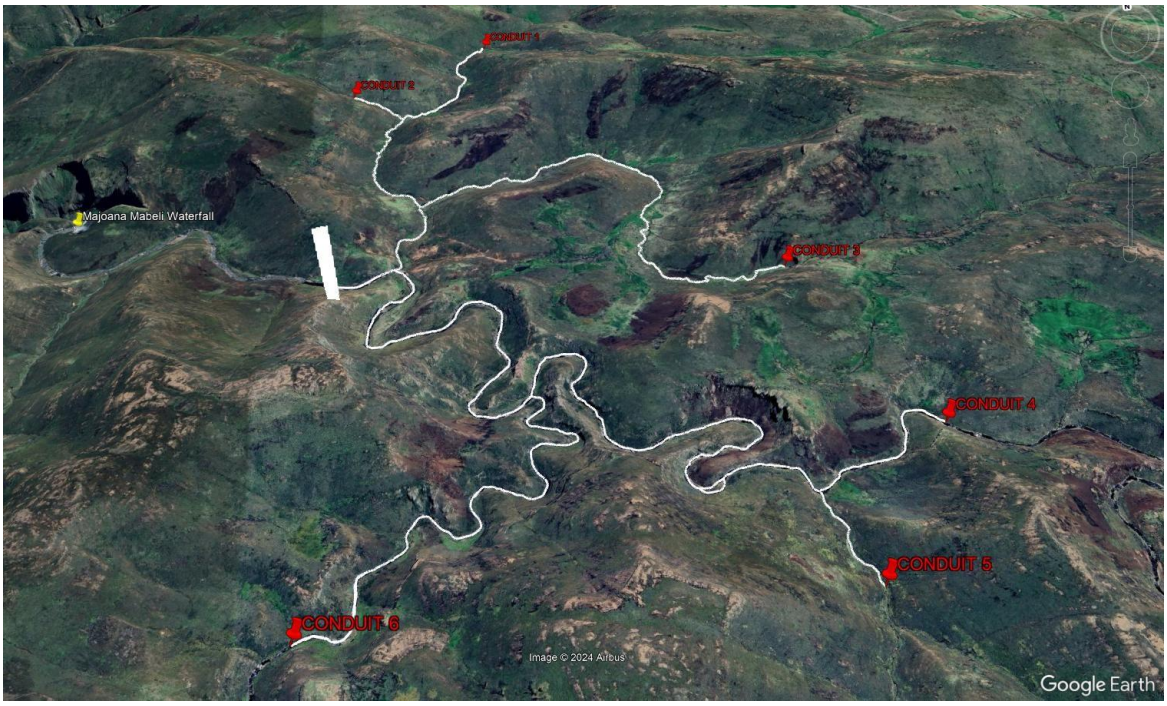

Figure 23 Anticipated installation arrangement of the conduits and the outlet

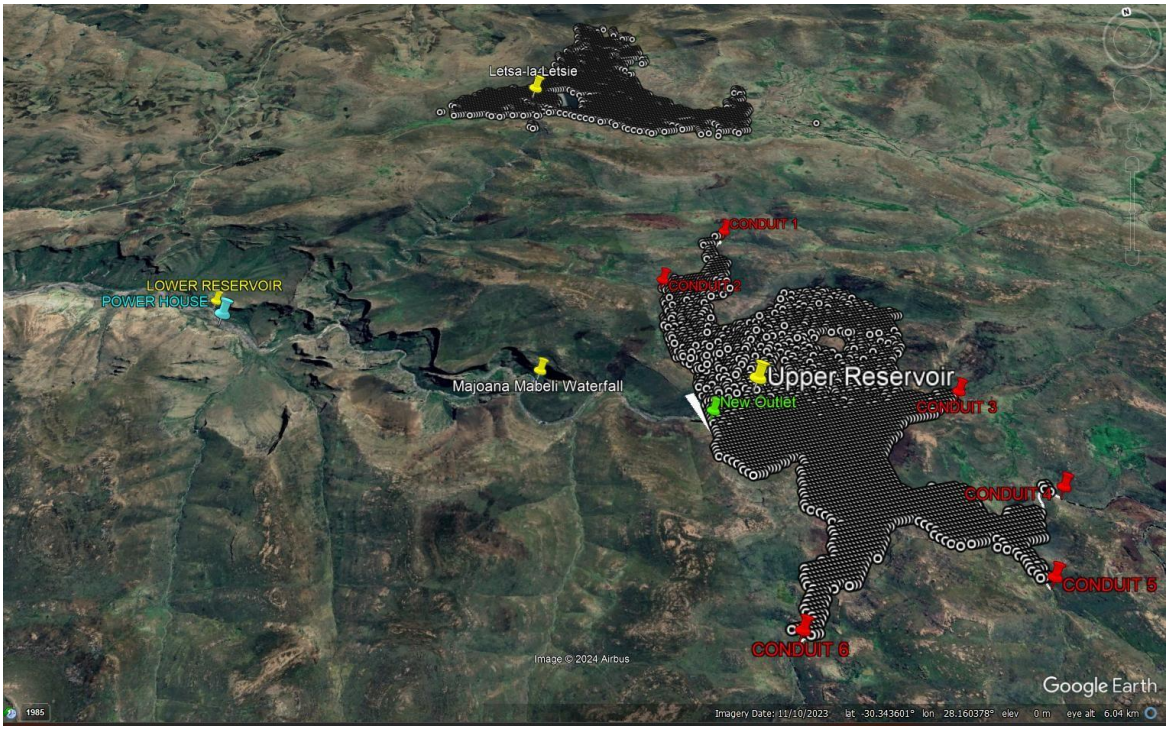

Figure 24 upper reservoir surface extend with the conduit's installation configuration beneath.

4. Results and Discussion

4.1 Hybrid System Simulation and Optimization

The hybrid setup in Figure 14, was simulated using HOMER as depicted in Figure 25. This system integrates solar, wind, and hydropower components. Solar and wind energy are harnessed to primarily operate solar pumps which elevate water from the lower to the upper reservoir, the secondary purpose of these resources is to supply power to the primary school in the area along with irrigation of the fields in the area. The pumped hydro storage aspect was represented in HOMER as a battery, with the capacity of the upper reservoir serving as the equivalent battery capacity. Figure 26 provides visual representations of the daily, yearly, and seasonal energy usage. The average daily energy consumption is 25,512 kWh, while the scaled daily energy use is 24,022.37 kWh. The average power consumption is 1,063 kW, and the scaled average power is 1,000.90 kW. The peak power consumption is 3,997.30 kW, with the scaled peak power being 3,763.90 kW. **Table 5** illustrates the daily energy consumption patterns, including the energy used for pumping, the school in the village of Ha Sera, and irrigation for nearby fields. **Table 6** presents the system's annual energy consumption profile, derived from the data in **Table 5**, using the HOMER software.

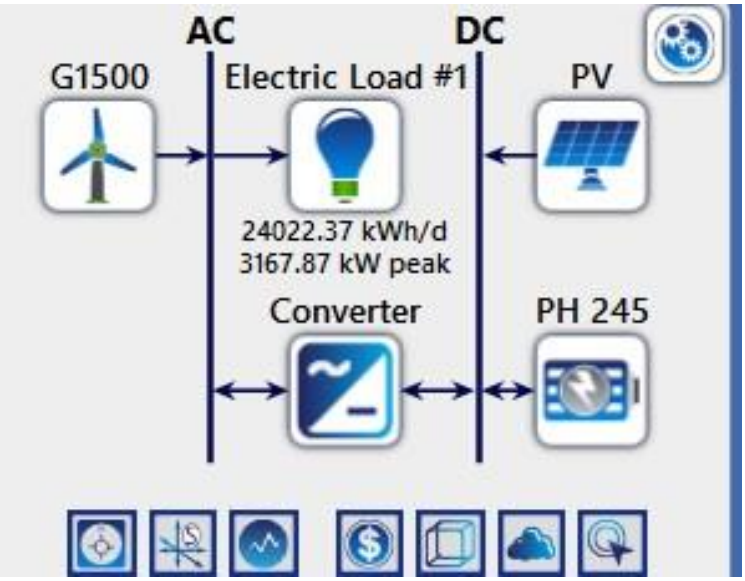

Figure 25 System Schematic of the Pumped storage system at Likhaebaneng River in Quthing District

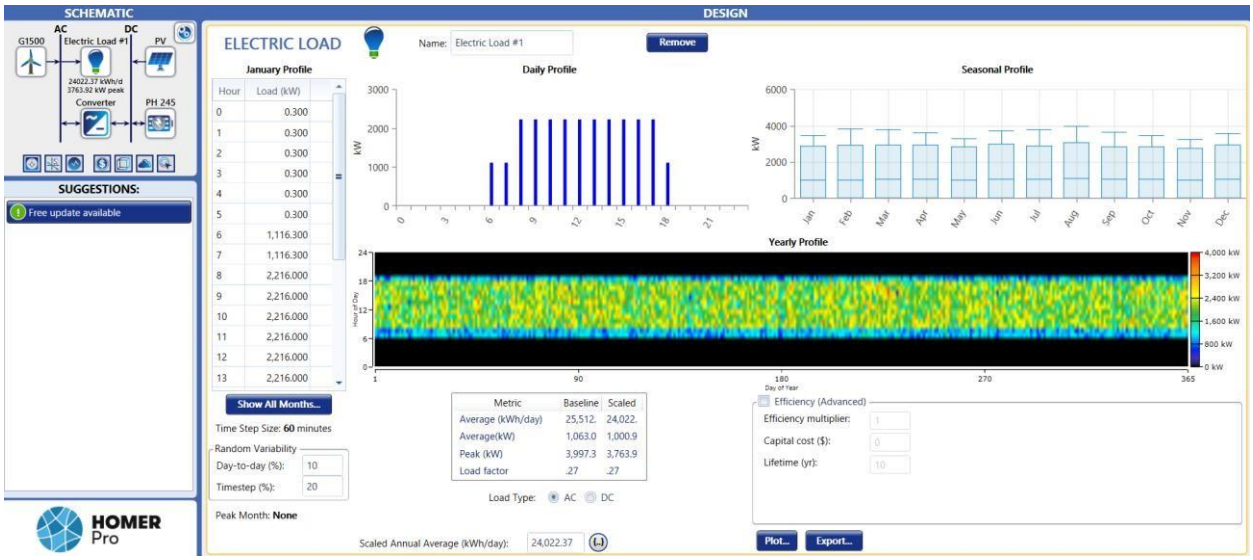

Figure 26 Daily, seasonal, and yearly load profile

Table 5 Daily Total Load in kW and in kWh

HOUR	Irrigation Load (kW)	Pumping Load (kW)	School Load (kW)	TOTAL Load (kW)	TOTAL Load (kWh)
0	0	0	0.3	0.3	3.6
1	0	0	0.3	0.3	3.6
2	0	0	0.3	0.3	3.6
3	0	0	0.3	0.3	3.6
4	0	0	0.3	0.3	3.6
5	0	0	0.3	0.3	3.6
6	80	1036	0.3	1116.3	13395.6
7	80	1036	0.3	1116.3	13395.6
8	80	1036	1100	2216	26592
9	80	1036	1100	2216	26592
10	80	1036	1100	2216	26592
11	80	1036	1100	2216	26592
12	80	1036	1100	2216	26592
13	80	1036	1100	2216	26592
14	80	1036	1100	2216	26592
15	80	1036	1100	2216	26592
16	80	1036	1100	2216	26592
17	80	1036	1100	2216	26592
18	80	1036	0.3	1116.3	13395.6
19	0	0	0.3	0.3	3.6
20	0	0	0.3	0.3	3.6
21	0	0	0.3	0.3	3.6
22	0	0	0.3	0.3	3.6
23	0	0	0.3	0.3	3.6

Table 6 Annual Load Profile

Yearly Load Data

Weekdays | Weekends

Hour	January	February	March	April	May	June	July	August	September	October	November	December
0	0.300	0.300	0.300	0.300	0.300	0.300	0.300	0.300	0.300	0.300	0.300	0.300
1	0.300	0.300	0.300	0.300	0.300	0.300	0.300	0.300	0.300	0.300	0.300	0.300
2	0.300	0.300	0.300	0.300	0.300	0.300	0.300	0.300	0.300	0.300	0.300	0.300
3	0.300	0.300	0.300	0.300	0.300	0.300	0.300	0.300	0.300	0.300	0.300	0.300
4	0.300	0.300	0.300	0.300	0.300	0.300	0.300	0.300	0.300	0.300	0.300	0.300
5	0.300	0.300	0.300	0.300	0.300	0.300	0.300	0.300	0.300	0.300	0.300	0.300
6	1,116.300	1,116.300	1,116.300	1,116.300	1,116.300	1,116.300	1,116.300	1,116.300	1,116.300	1,116.300	1,116.300	1,116.300
7	1,116.300	1,116.300	1,116.300	1,116.300	1,116.300	1,116.300	1,116.300	1,116.300	1,116.300	1,116.300	1,116.300	1,116.300
8	2,216.000	2,216.000	2,216.000	2,216.000	2,216.000	2,216.000	2,216.000	2,216.000	2,216.000	2,216.000	2,216.000	2,216.000
9	2,216.000	2,216.000	2,216.000	2,216.000	2,216.000	2,216.000	2,216.000	2,216.000	2,216.000	2,216.000	2,216.000	2,216.000
10	2,216.000	2,216.000	2,216.000	2,216.000	2,216.000	2,216.000	2,216.000	2,216.000	2,216.000	2,216.000	2,216.000	2,216.000
11	2,216.000	2,216.000	2,216.000	2,216.000	2,216.000	2,216.000	2,216.000	2,216.000	2,216.000	2,216.000	2,216.000	2,216.000
12	2,216.000	2,216.000	2,216.000	2,216.000	2,216.000	2,216.000	2,216.000	2,216.000	2,216.000	2,216.000	2,216.000	2,216.000
13	2,216.000	2,216.000	2,216.000	2,216.000	2,216.000	2,216.000	2,216.000	2,216.000	2,216.000	2,216.000	2,216.000	2,216.000
14	2,216.000	2,216.000	2,216.000	2,216.000	2,216.000	2,216.000	2,216.000	2,216.000	2,216.000	2,216.000	2,216.000	2,216.000
15	2,216.000	2,216.000	2,216.000	2,216.000	2,216.000	2,216.000	2,216.000	2,216.000	2,216.000	2,216.000	2,216.000	2,216.000
16	2,216.000	2,216.000	2,216.000	2,216.000	2,216.000	2,216.000	2,216.000	2,216.000	2,216.000	2,216.000	2,216.000	2,216.000
17	2,216.000	2,216.000	2,216.000	2,216.000	2,216.000	2,216.000	2,216.000	2,216.000	2,216.000	2,216.000	2,216.000	2,216.000
18	1,116.300	1,116.300	1,116.300	1,116.300	1,116.300	1,116.300	1,116.300	1,116.300	1,116.300	1,116.300	1,116.300	1,116.300
19	0.300	0.300	0.300	0.300	0.300	0.300	0.300	0.300	0.300	0.300	0.300	0.300
20	0.300	0.300	0.300	0.300	0.300	0.300	0.300	0.300	0.300	0.300	0.300	0.300
21	0.300	0.300	0.300	0.300	0.300	0.300	0.300	0.300	0.300	0.300	0.300	0.300
22	0.300	0.300	0.300	0.300	0.300	0.300	0.300	0.300	0.300	0.300	0.300	0.300
23	0.300	0.300	0.300	0.300	0.300	0.300	0.300	0.300	0.300	0.300	0.300	0.300

4.2 Hydrograph for Likhaebaneng River and Flow Duration Curve (FDC)

The streamflow data for the gauged river, specifically the Quthing River at Hoko, was acquired from the Department of Water Affairs (DWA). The hydrograph in Figure 15 provides a more comprehensive insight into the typical patterns of Likhaebaneng River flow over a 39-year

period. Peak flows occur in the summer months, coinciding with Lesotho's rainy season, whereas the lowest flows are observed in winter. December records the highest flow levels, while August consistently registers the lowest flow rates. This data was utilized to establish the FDC for Likhaebaneng River. Following the determination of the FDC, the flow rate at Q_{50} was determined to be 0.3 m^3 /s and this flow rate was then used as the design flow rate. The FDC is visually represented in Figure 16.

4.3 Catchment areas and flow rates

The study areas' catchment areas were identified utilizing GIS and WMS. A total of four catchment areas were computed to ascertain the flow rate of the Likhaebaneng River; these areas are essential for determining the potential power generation of the planned PHES. The initial catchment area analysed was the Quthing River at Hoko, measuring 600 km^2 as shown in Figure 27. This is followed by the catchment area at the abstraction point, which was measured to be 198.74 km as illustrated in Figure 28. The catchment area before the confluence of the two rivers, which is shown in Figure 29, was then evaluated as 140.41 km^2. The flow rate of 0.3 m^3/s was determined from the flow duration curve in Figure 16 at percentage exceedance of 50 percent.

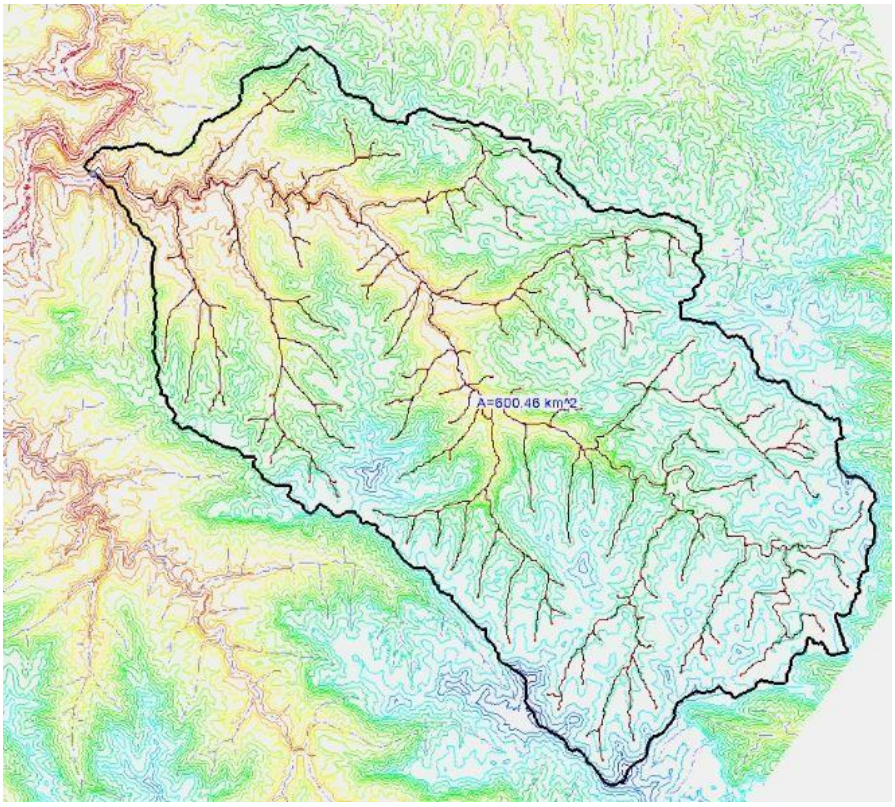

Figure 27 Quthing River Catchment Area

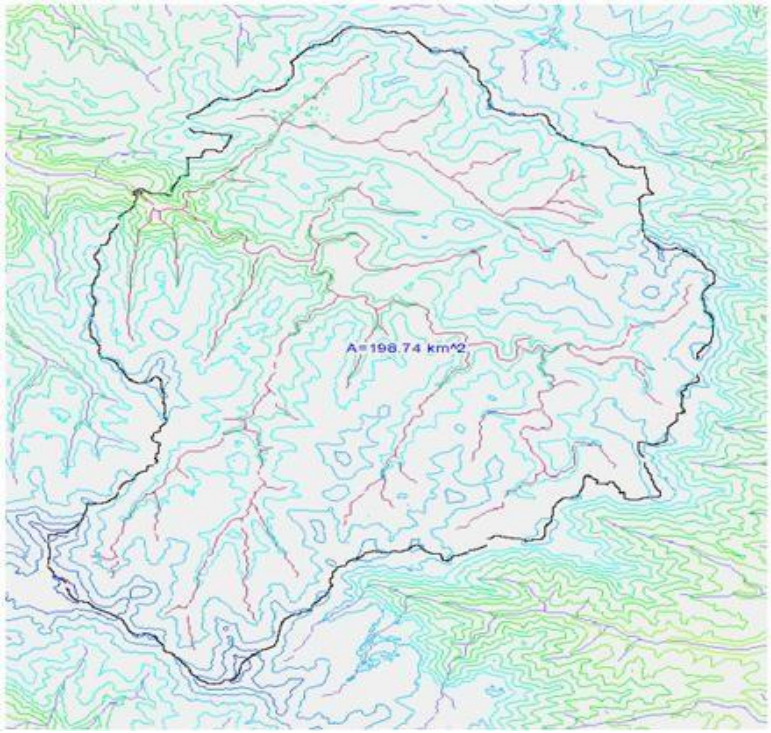

Figure 28 Catchment Area at the abstraction point

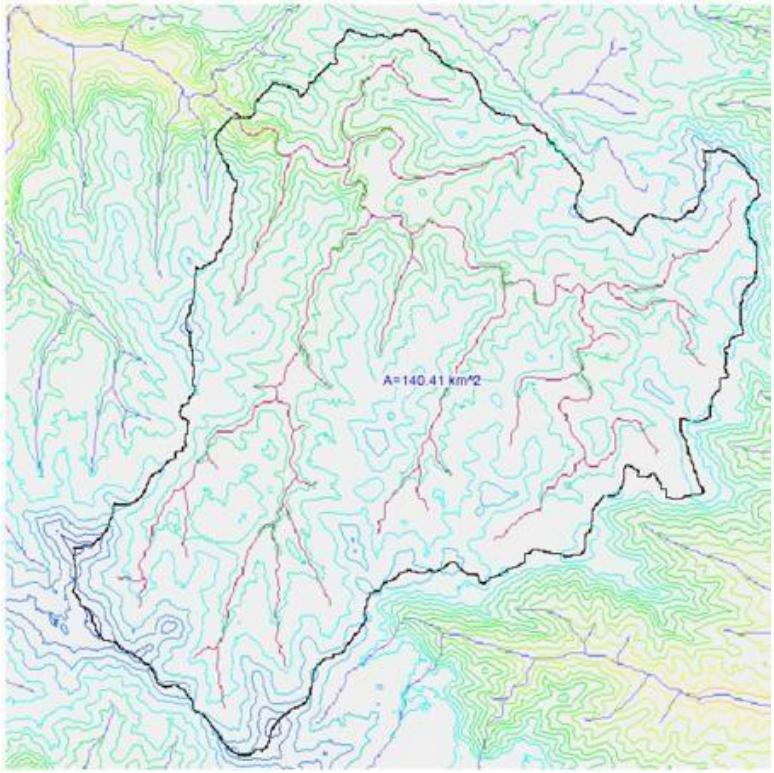

Figure 29 Catchment Area before the confluence

4.4 Modelling a pumped storage as battery in HOMER

The data from

Table 4 was used as input for modelling a pumped storage system as a battery in HOMER, with the results presented in Figure 30. Using Equation 4-1, the annual efficiency of the pumped storage was determined. The input energy was calculated to be 2,130,818 kWh per year, and the output energy was 1,502,848 kWh per year, resulting in losses of 641,447 kWh/year. Consequently, the efficiency was found to be 70.53%. The system's annual throughput is 1,796,247 kWh/year, with a life expectancy of 25 years and a projected lifetime throughput of 44,906,168 kWh.

$$\eta = \frac{1,502,848\ kWh/yr}{2,130,818\ kWh/yr} x\ 100 = 70.53\ \%$$ *Equation 4-1*

Figure 30 Representation of a pumped hydropower plant as an equivalent battery.

4.5 Upper Reservoir size Computation

The upper reservoir extent calculation involved identifying all points within the catchment area using GIS and WMS softwares. Out of a total number of points within the reservoir extent, negative points that were found signified that they are located beyond the reservoir's coverage area. In other words, these points were representing the region extending beyond the reservoir's full supply level, rendering that area non-usable for the reservoir. Consequently, the area covered by these negative points was not taken into consideration hence these points are not captured along with positive points in Figure 31. On the other hand, the 619 points that were identified as positive, displayed in Figure 31, indicated that the area encompassed by these points either falls within the reservoir's full supply level or extent downstream from the reservoir. The numbers of both positive and negative points are both displayed in Figure 32; the positive points cover the usable area within the catchment area while the negative points cover the non-usable area within the catchment area. The number of points that represent positive values are indicated by a black arrow, while those representing negative values are marked with a red arrow. The positive points, which are the ones that determine the size of the reservoir, were selected through the “selection by attributes” function in GIS. The size of the upper reservoir was then determined as illustrated by the black circled area in Figure 33. Once the capacity of the reservoir had been ascertained, it was subsequently visualized in Google Earth Pro to precisely depict the reservoir's location, as shown in Figure 34.

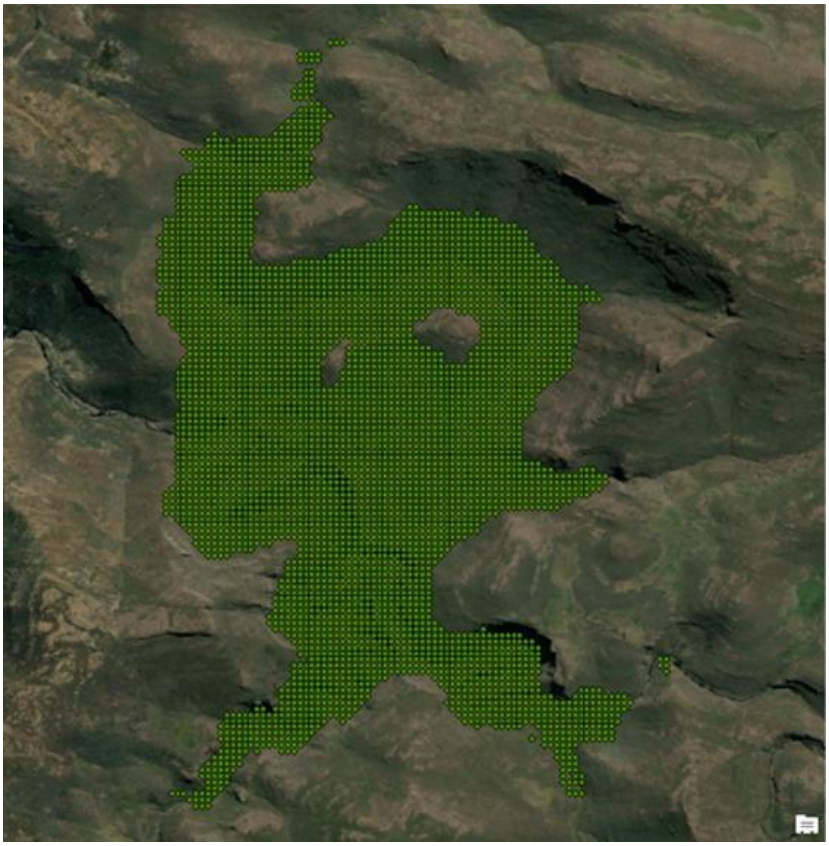

Figure 31 Positive points within the upper reservoir

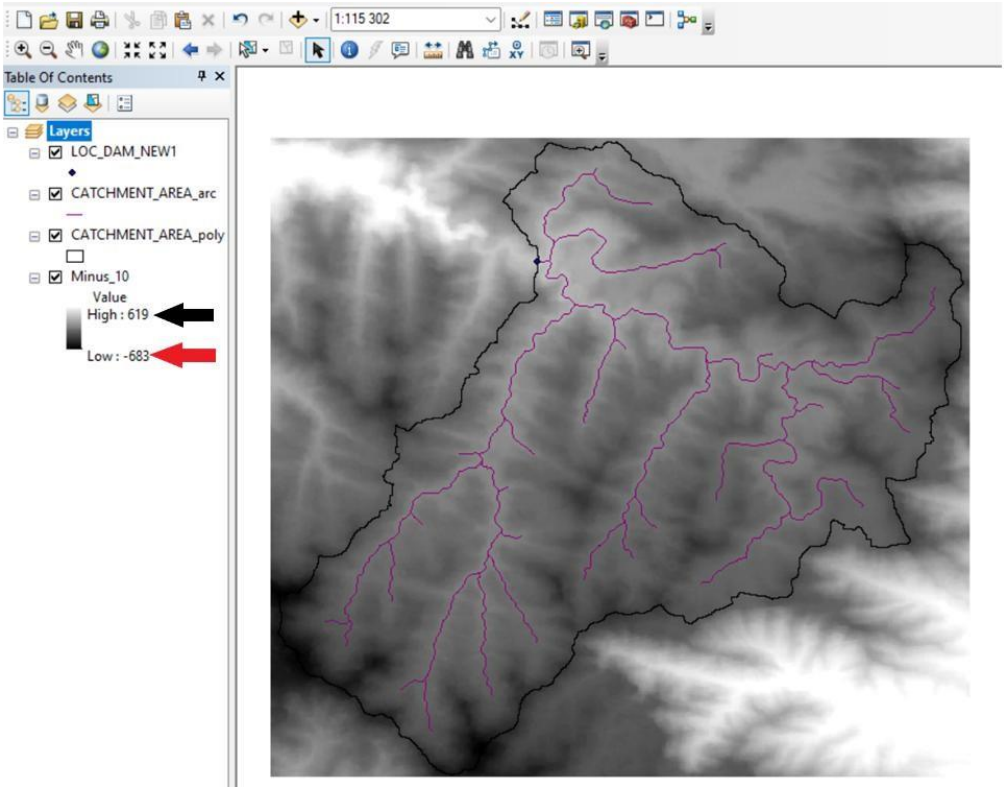

Figure 32 Negative and Positive points within the upper catchment area

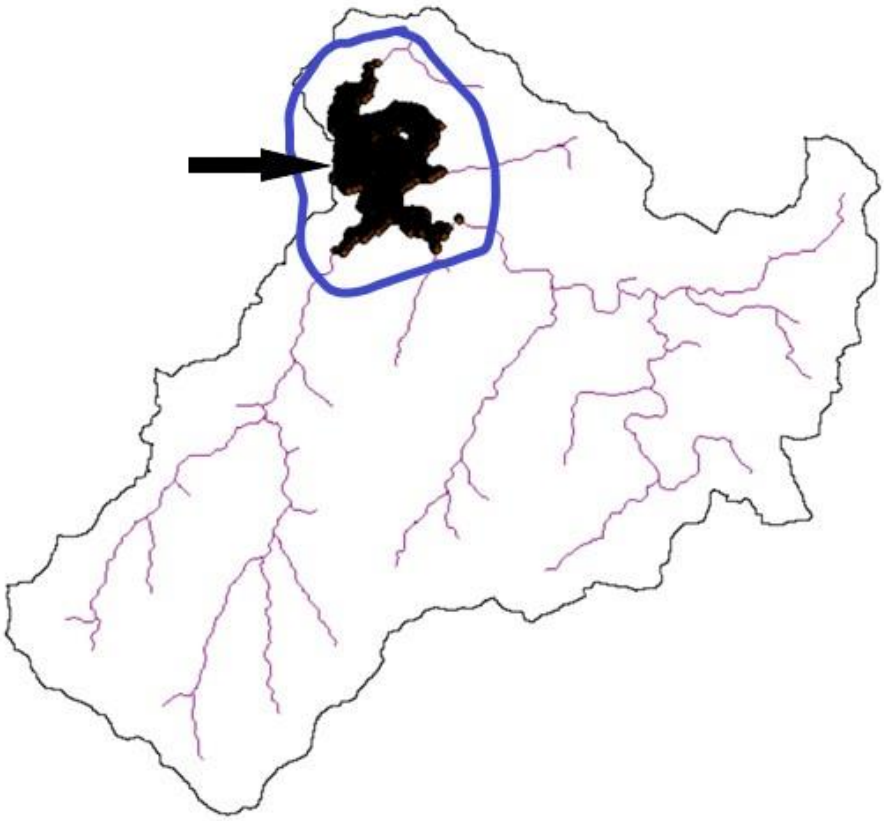

Figure 33 Upper reservoir size / capacity

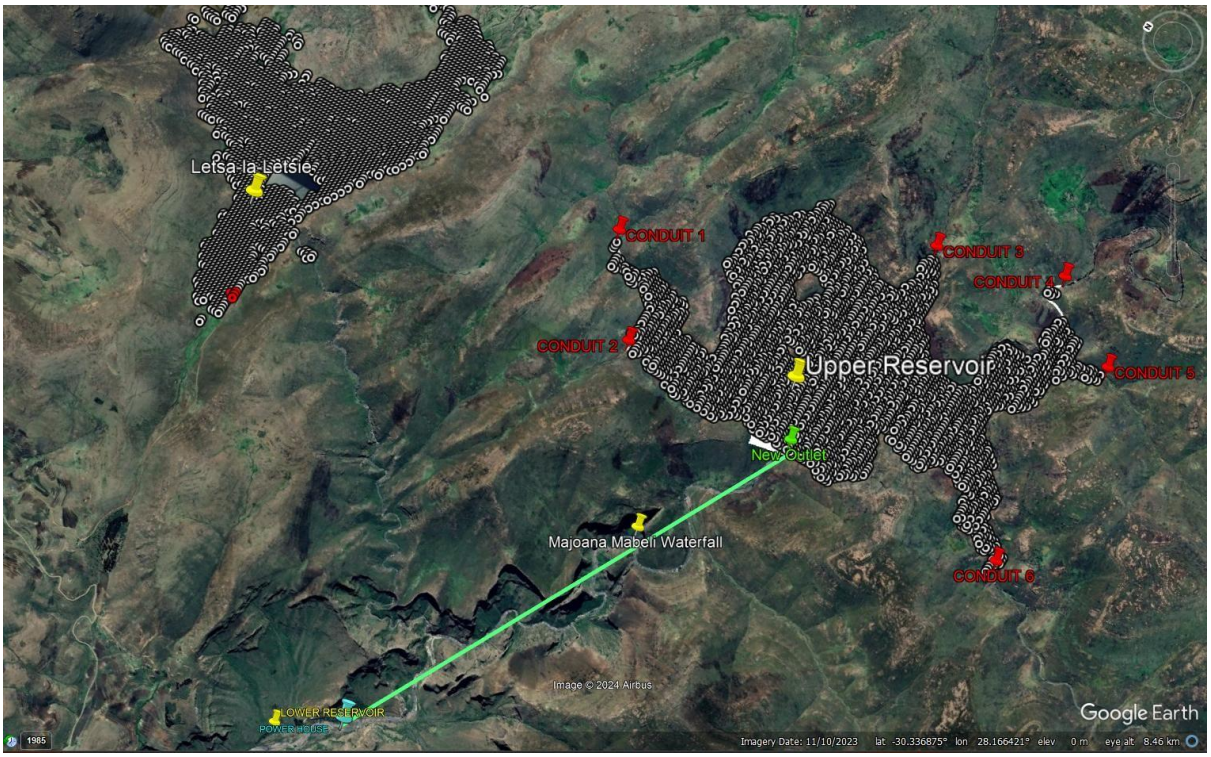

Figure 34 Upper Reservoir Location

4.6 Upper reservoir volume computation

The determination of the upper reservoir's volume involved a GIS-based process, following a series of steps. Firstly, positive points within the reservoir's full supply level were loaded into GIS. The attributes table was then accessed to ascertain the reservoir's depth, using these points and the attribute table depicted in Figure 35. The column labelled 'grid code' in the attribute table denotes the reservoir depth, and the maximum depth was identified as 131 meters as illustrated in Figure 36

The summation of all depth values in the 'grid_code' column provides the total depth of the reservoir. In Figure 36, the cumulative depth was computed as 204273 meters. The distances between successive positive points within the catchment area were measured to determine the length and width of the reservoir, resulting in values of 27.412007 and 31.602726 meters, respectively. Utilizing Equation 3-6, the total volume of the reservoir was then calculated as:

Total reservoir volume = 204273 m x 27.412007 m x 31.602726 m = 176,960,504 m^3 = 1.77 M cubic meters.

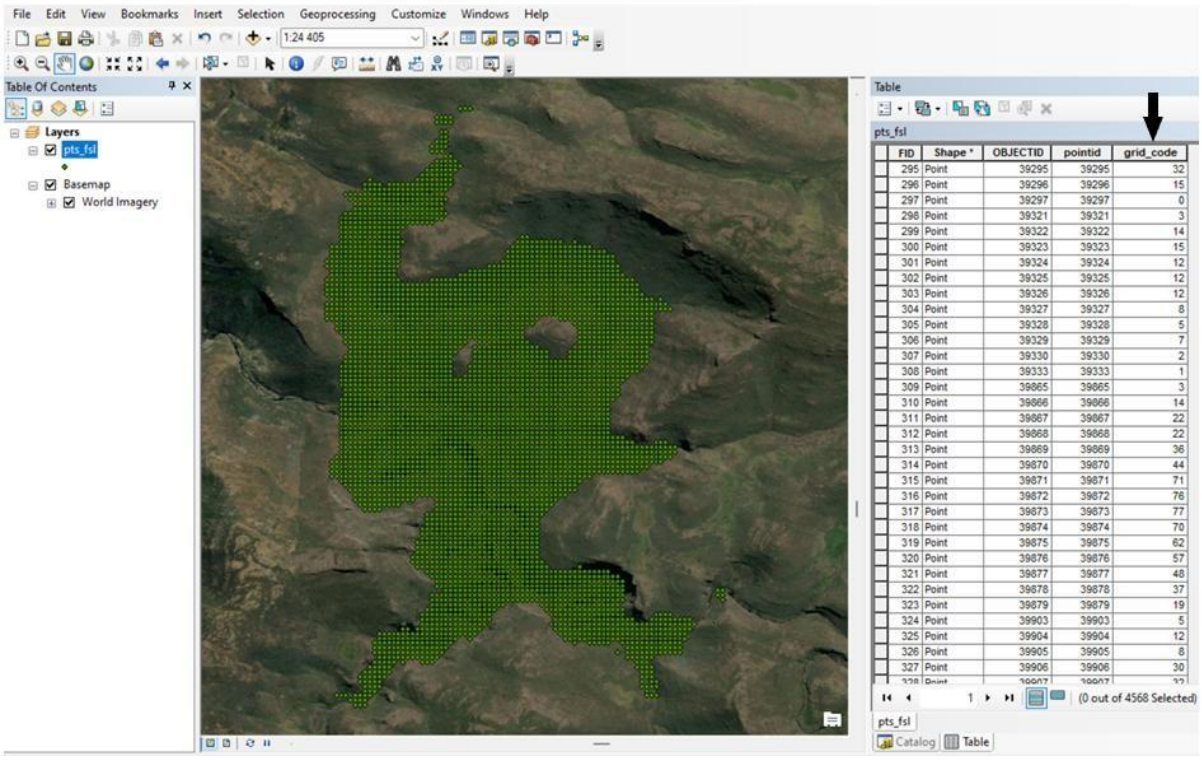

Figure 35 Attribute Table and the full supply level points

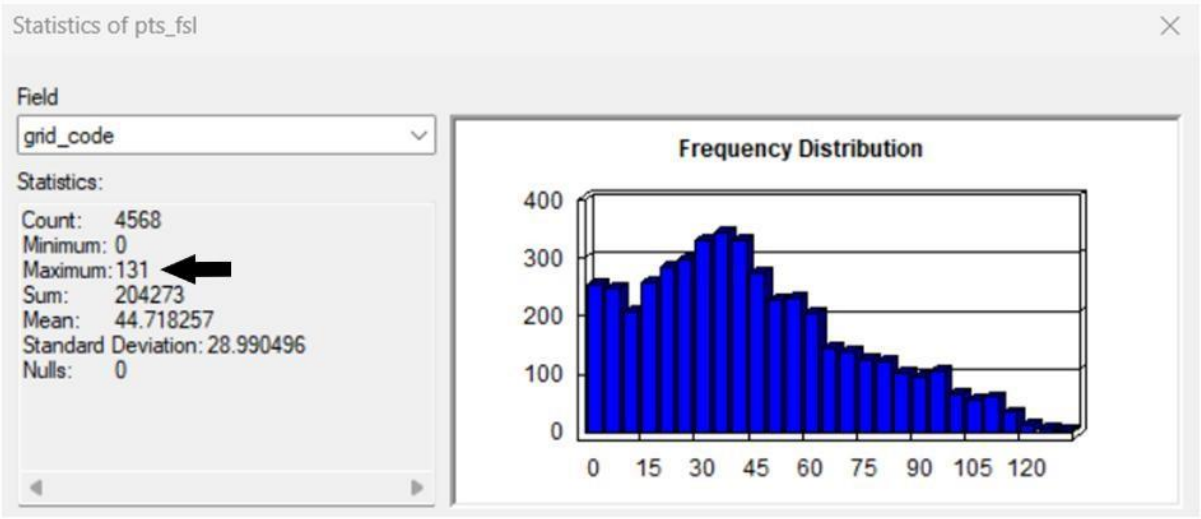

Figure 36 Statistics table showing the minimum and maximum depth of the upper reservoir

4.7 Pump selection

The comparison between two Lorentz pumps, namely the G200 – 244 and G125 - 404, led to the selection of the G200 – 244 for pumping water from a lower to an upper reservoir. This choice was primarily based on the G200 – 244 requiring fewer pumps when connected in both series and parallel configurations. The specifications and pump chart for the G200 – 244 are presented in Figure 18 and Figure 19 respectively.

4.7.1 Pumps connected in parallel

As per the Equation 3-7, the G200 – 244 necessitates around two pumps to be linked in parallel to achieve a water pumping rate of 0.3 m^3/s. In contrast, the G125 – 404 requires about four units connected in parallel to attain the same water pumping rate. When employing G125 – 404, a total of eight cascading reservoirs and 32 pumps are needed, whereas for G200 – 244, the requirement is for 14 cascading reservoirs, totalling 28 pumps. Consequently, it was more economical to utilize the G200–244 pumps in the cascading system for water pumping. The specifications and the pump chart for G200 – 244 are displayed in Figure 18 and Figure 19 respectively, while the G125 – 404 specifications and pump chart are displayed in Figure 20 and Figure 21 respectively.

The number of G200 – 244 pumps is

$P_p = \frac{0.3}{0.14}$ = *2.1 pumps (approximately 2 pumps connected in parallel*

The number of G125 – 404 pumps is

$P_p = \frac{0.3}{0.07}$ = 4.1 pumps (approximately 4 pumps connected in parallel) Where P_p represents pumps in parallel

4.8 Cascading Reservoirs Determination

Following the determination of the volume for the upper reservoir, the next step involved assessing the number of cascading reservoirs required to fulfil the objectives of the project. The number of cascading reservoirs was determined using Equation 3-8.

N_{cr} (G200 – 244) = $\frac{301\ m}{22\ m}$ = 13.7 reservoirs (14 cascading reservoirs)

It was determined that there are 14 cascading reservoirs, each equipped with 2 pumps connected in parallel to ensure sufficient water is pumped to the upper reservoir. This brings the total number of pumps in the system to 28.

4.9 Pumps Power supply

The objective of the project is to harness renewable resources that are located along the Likhaebaneng River to operate all the pumps. To address the issue of transmission losses stemming from long power lines, every reservoir will be powered autonomously by solar panels and a wind turbine situated nearby. This strategic placement of energy sources near the reservoirs will eliminate the necessity for lengthy transmission cables and the consequent high transmission losses. The illustration of this arrangement is shown in Figure 2 where CR stands for Cascading Reservoir and PH stands for Power House.

HOMER and GIS software were utilized to assess the adequacy of renewable resources within the designated study area. GIS was used to obtain the results in Figure 37 which depict the study area. It showcases cells representing solar power availability in kilowatts per square meter per month (kW/m^2/month). Each cell is uniquely named and contains information regarding the energy potential it holds. For demonstration purposes, one cell that was randomly selected

had X coordinates of 281708 and Y coordinates of 303625, with a solar power potential of 136.74 kW/m^2/month. This power value is indicated in the "grid_code" column of the adjacent table alongside the cells. Figure 38 is a chart depicting the solar power potential of the same cell. These cells span the entirety of the study area and beyond, hence it can be known exactly where the resources are optimal and solar collectors and wind turbines can be positioned strategically to maximise energy harvesting. The findings depicted in Figure 39 illustrate the monthly mean data of solar global horizontal irradiance (GHI), whereas Figure 40 displays the monthly average data of wind speed within the research site, both sourced from HOMER software.

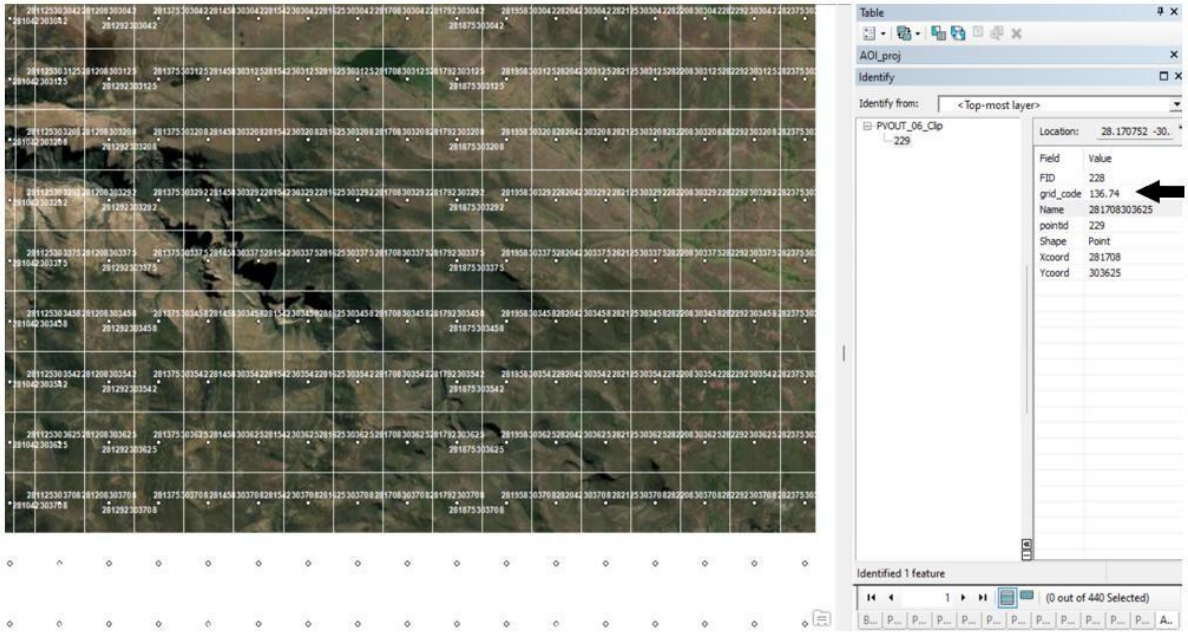

Figure 37 Cells depicting power availability in the study area

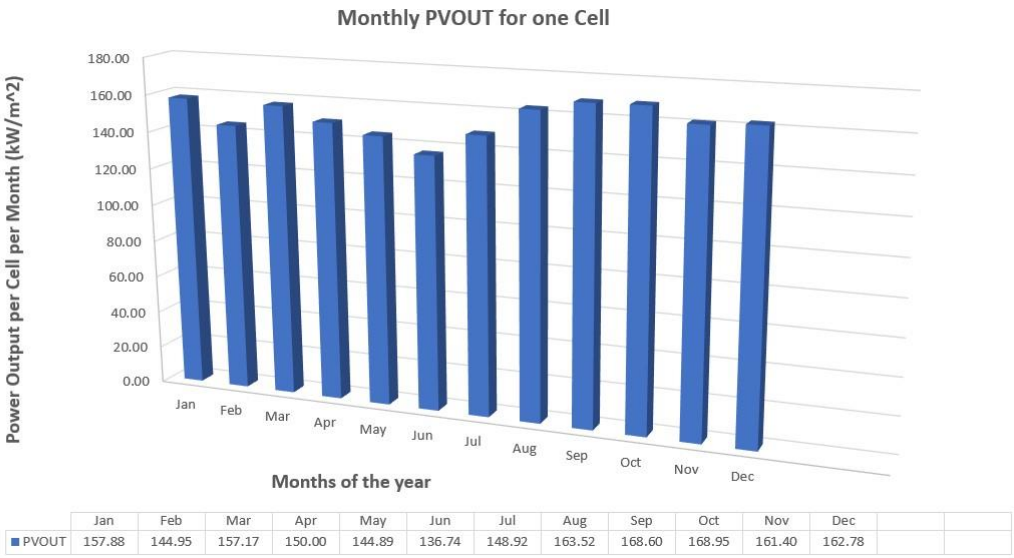

	Jan	Feb	Mar	Apr	May	Jun	Jul	Aug	Sep	Oct	Nov	Dec
PVOUT	157.88	144.95	157.17	150.00	144.89	136.74	148.92	163.52	168.60	168.95	161.40	162.78

Figure 38 Monthly PVOUT for one specific cell with optimal solar resources

4.10 HOMER Renewable resources

The data extracted from HOMER, as shown in Figure 39, reveals a global horizontal irradiation average of 5.19 kWh/m^2/day annually, accompanied by an average clearness index of 0.595.

Figure 40 demonstrates that the monthly average wind speed peaks notably in May and June, while it reaches its lowest levels in January and February. This mutual interplay between the two resources is evident: during periods of diminished wind speed, solar resources are at their zenith, whereas wind speeds are at their peak when solar resources are at their nadir. To be more precise, wind resources peak in June with an average wind speed of 5,580 m/s, while solar resources are at their lowest during the same month, with June's average solar irradiation recording 3.168 kWh/m²/day, the lowest of any month in the year. This inverse relationship between the two resources is advantageous because using both will complement each other and ensure continuous production of electrical energy. The average wind speed measures at 4.86 m/s, surpassing the typical threshold of 4 m/s necessary for wind power systems to be financially viable [71]. Furthermore, its distribution adheres to the Weibull function with a parameter value of k = 2.

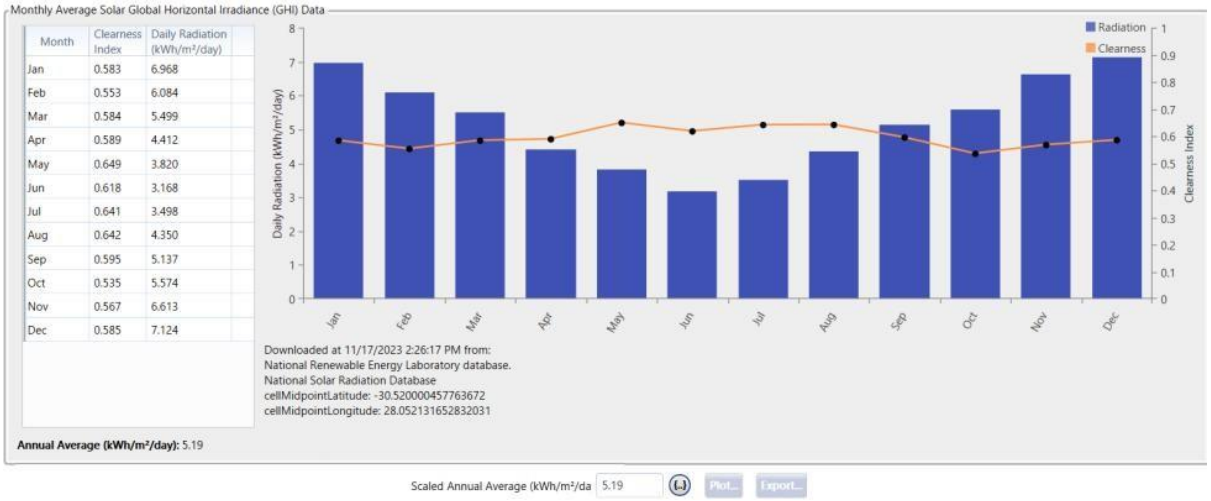

Figure 39 Monthly Average Solar Global Horizontal Irradiance (GHI) Data in Likhaebaneng river in the Quthing District

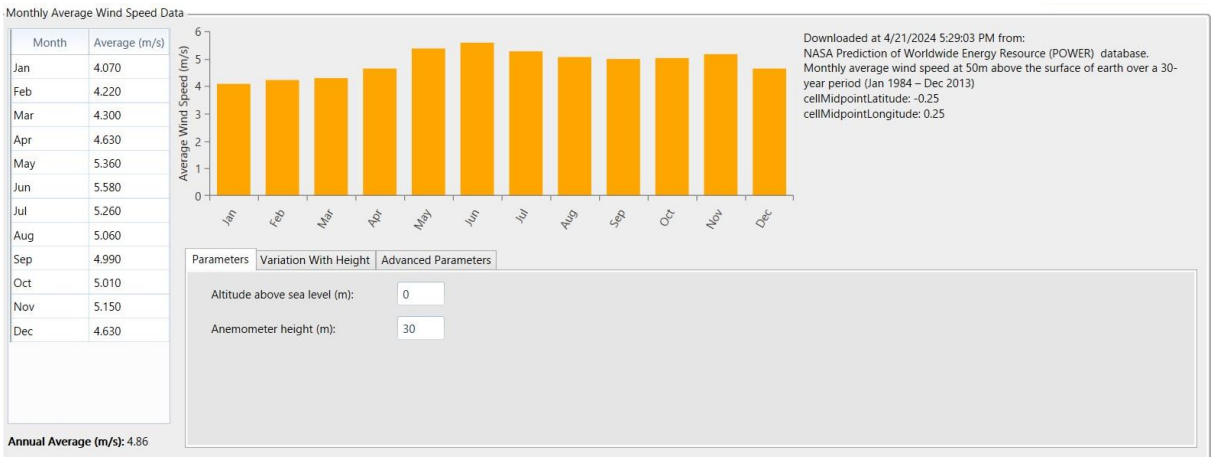

Figure 40 Monthly Average Wind Speed Data in Likhaebaneng river in the Quthing district

4.10.1 HOMER Optimised results

The HOMER simulation generates a roster of viable design alternatives or system configurations, ordered by their minimal total net present cost (NPC). Analysing each attainable system configuration permits the assessment of both economic and technical advantages, encompassing metrics like the levelized cost of energy (LCOE) and the proportion of renewable energy utilized.

For the present system, HOMER suggested optimal system configurations starting with the most cost effective and ending with the least cost effective as displayed in Figure 41. For instance, the most cost-efficient configuration involving a combination of a wind turbine, solar resources, and water storage, displays a Net Present Cost (NPC) of $46.48 million, with a Cost

of Energy (COE) at $0.2053 per kilowatt-hour (kWh), or M3.95 per kWh, and an initial investment of $29.29 million. Conversely, the second proposed setup which incorporates solar resources and water storage emerges as the second most economically viable option, with an NPC of $55.58 million, a COE of $0.2454, and an initial capital investment of $35.83 million. The last system is comprised of wind resources and water storage with the NPC of $80.9, a COE of $0.358, and the initial capital investment of $47.8 million.

Figure 42 depicts the electrical output of the system encompassing energy production, load consumption, and surplus electrical generation. The system annually generates 8,074,658 kWh from solar resources, constituting 58.2% of the total production. Additionally, 5,797,867 kWh per year is generated from wind resources, accounting for 41.8% of the system's total annual energy production of 13,872,525 kWh. The consumption amounts to 8,764,589 kWh per year, resulting in an excess energy production of 28.9 %. In Figure 43, the annual production of PHES reaches 2,228,537 kWh, with an annual input energy of 2,648,308 kWh, resulting in an efficiency of 84.15 %, while Figure 44 shows the maximum PV Power output of 4,568 kW operating for 4,380 hrs/yr. The wind maximum power output is displayed in Figure 45. The maximum wind power output is 3,000 kW operating for 5,808 hrs/yr.

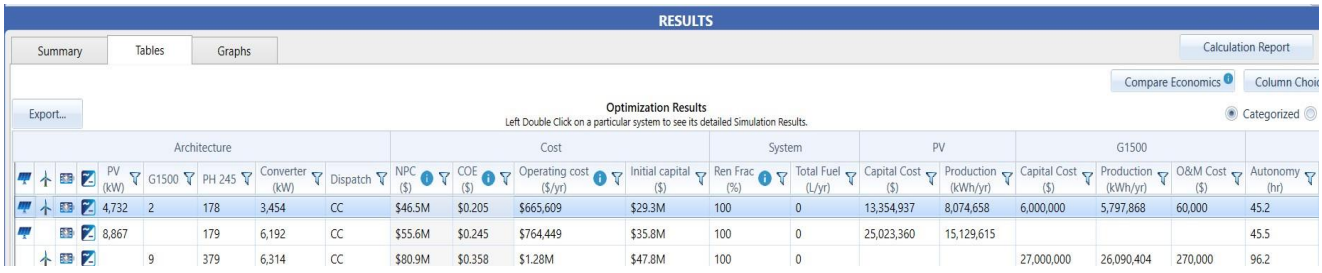

Figure 41 HOMER optimised results

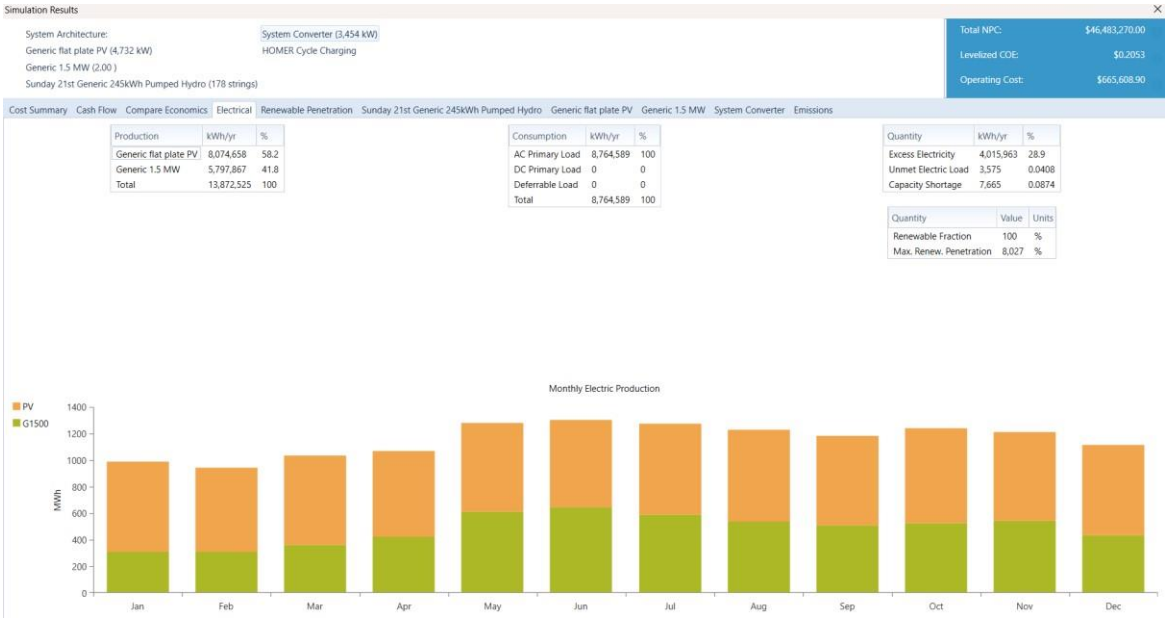

Figure 42 Solar and Wind energy production and consumption

Figure 43 Energy Production of PHES System

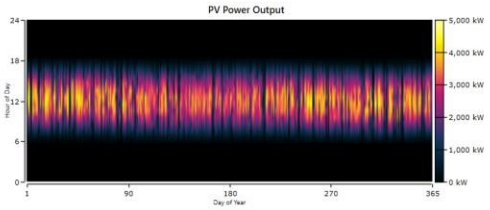

Figure 44 PV Power output

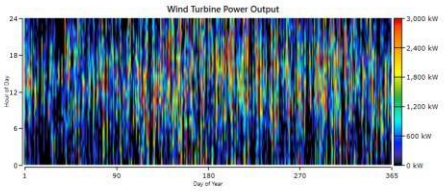

Figure 45 Wind Turbine Power Output

4.11 Rainfall Patterns in the study area

The study area's rainfall patterns were analysed to ensure sufficient water resources for power generation. January typically sees the most rainfall while July has the least rainfall as shown in Figure 46. From 2001 to 2021, the average rainfall in January was 130.82 mm compared to 15.17 mm in July. These figures are detailed in Table 7. Additionally, Figure 46 indicates that water resources are quite low from May to September, potentially preventing the flow rate from

reaching 0.3 m³/s during this period. According to Figure 39, solar resources are also at their lowest from May to August, aligning with the low water resources. However, Figure 40 reveals that wind speeds peak during this same period, effectively compensating for the diminished water and solar resources.

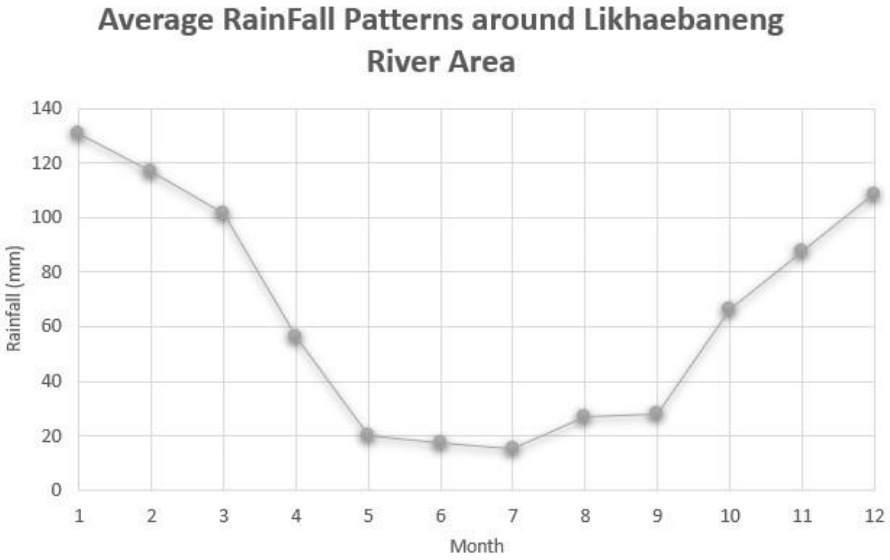

Figure 46 Rainfall Patterns around the Likhaebaneng River

Table 7 Average Monthly Rainfall Patterns in Likhaebaneng River (2000 - 2021)

Yearly	2000	2001	2002	2003	2004	2005	2006	2007	2008	2009	2010	2011	2012	2013	2014	2015	2016	2017	2018	2019	2020	2021	Monthly
Annual		1009.3	851.297	503.653	821.39	606.683	1065.79	617.54	685.067	902.56	903.946	901.979	889.227	693.232	771.161	564.231	779.277	716.758	746.581	737.671	757.296		776.232
Jan		98.513	152.364	84.9242	135.271	131.221	181.845	76.8469	102.205	138.933	194.075	182.667	115.653	139.615	123.718	151.144	156.98	137.527	142.086	69.9321	100.958	205.677	130.824
Feb		98.6578	72.2032	80.5979	118.754	87.9663	163.945	40.3738	94.0231	200.485	115.138	153.275	134.11	80.2918	122.118	61.8132	102.792	190.29	100.63	156.506	168.754	115.231	117.136
Mar		103.12	94.1144	78.9172	143.046	85.3451	81.7213	69.3091	84.9219	84.7573	89.395	144.601	119.48	99.9816	94.9467	103.363	74.8661	34.5009	168.508	190.258	88.8451	49.7065	101.7
Apr		92.9558	36.9128	37.4266	40.1226	43.1215	76.1696	54.8448	49.3864	33.1186	48.3124	67.4909	23.1955	40.1674	36.6345	41.5132	56.3944	34.916	86.0423	123.435	103.083	34.393	56.2622
May		22.0215	93.6955	19.4764	0.52526	24.5221	27.5785	3.41442	19.4011	8.38511	6.02637	35.0036	9.04189	12.3414	3.55649	4.03911	29.1367	37.4447	26.4223	15.2963	0.94769	10.7008	19.9138
Jun	7.76851	16.3361	16.0413	0.14199	8.4027	6.42806	2.57444	28.7582	42.4975	38.6357	38.617	31.0882	59.2907	4.95067	4.3127	34.6676	3.39989	8.5033	2.25757	0.04948	0.69172	26.548	17.3822
Jul	2.48219	7.76426	35.9676	1.10631	14.2239	0.23145	2.67897	2.18412	0.4266	11.1133	0.02051	38.9016	40.3211	4.35852	1.03912	29.3309	96.4261	0.74728	15.23	0.80691	0.55694	0.64549	15.1718
Aug	2.51033	51.4719	106.6	22.9576	18.962	31.9467	93.223	12.0464	12.0924	27.4183	0.23275	15.3196	33.0205	5.6869	18.0408	7.98806	18.2171	1.84409	55.9533	1.20467	1.38218	28.7679	26.7804
Sep	35.7355	37.3641	45.9327	30.7651	76.9492	13.4206	32.2087	33.4836	10.5183	4.48836	10.8218	7.48854	68.9708	42.2357	13.398	34.997	28.1929	8.91713	25.585	13.6423	21.192	39.2084	28.0286
Oct	59.6682	97.6329	26.1515	24.0118	55.6224	73.6696	137.163	104.311	27.2141	195.366	69.7823	37.095	99.4004	57.8028	44.794	36.9471	42.1207	93.5647	24.7417	7.93837	72.7417		66.4035
Nov	102.122	214.569	39.4712	65.9767	86.7071	92.2395	140.719	96.3523	100.935	96.1523	128.884	41.8048	49.6572	90.7899	148.169	29.1678	109.062	79.7757	32.3299	35.3585	79.961		87.9041
Dec	116.697	168.893	131.842	57.3509	122.803	16.5711	125.963	95.6154	141.446	63.707	202.641	147.244	137.086	115.01	160.433	29.2596	61.6886	88.7269	66.7951	123.243	118.183		108.725

4.12 Penstock Length

The length of the penstock was determined by utilizing the measuring feature within Google Earth Pro, yielding a measurement of 4.38 kilometres. This information is depicted in Figure 47. Additionally, the diameter was determined to be 0.529 meters as indicated in Equation 3-9.

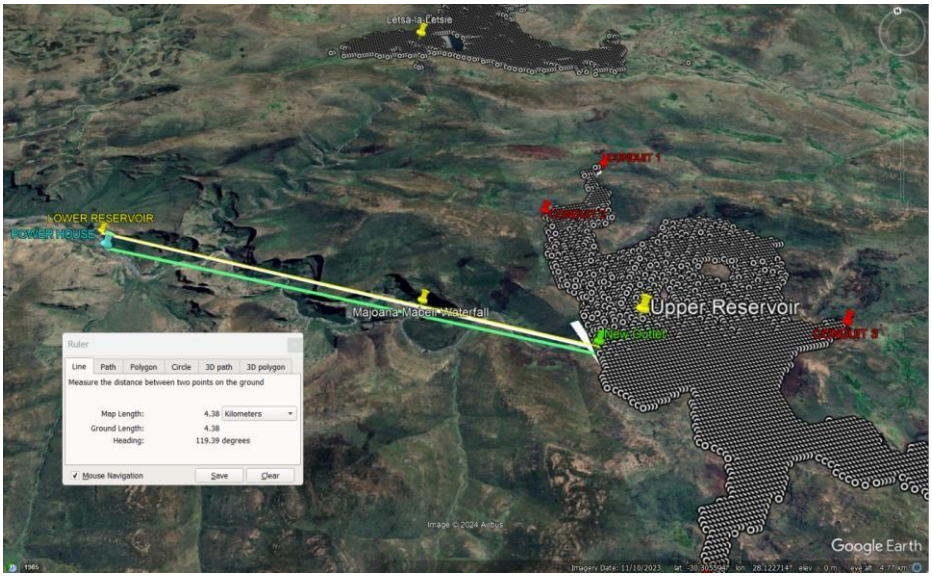

Figure 47 Penstock Length

4.13 Static head

Static head is a combination of straight run head losses and fitting head losses.

1.6.5.1 Straight run head loss

Equation 3-10 was employed to compute the straight run head losses within the system. In the initial design, the water velocity was assumed to be 1.5 m/s. The average daily temperature in the study area was approximately 10 ˚C (9.72 ˚C). The dynamic viscosity value, obtained from Table 8, was determined as 1.307 x 10^{-3}. The Reynolds number (Re) was calculated using Equation 3-11 and found to be 610. Referring to Table 9, since Re is less than 2000, Equation 3-12 was utilized to determine the friction factor of the penstock.

$$D = \sqrt{\frac{4x0.3}{\pi x1}} = 0.529 \text{ m}$$

$$h_s = \frac{0.10492 \; x \; 4340m \; 1.5^2}{2 \; x \; 0.529 \; x \; 9.81} = 89 \; m$$

$$Re = \frac{1.5 \; x \; 0.529}{1.307 \; x \; 10^{-3}} = 610$$

$$f = \frac{64}{610} = 0.10492$$

Table 8 Physical Properties of Water (SI Units

Temperature (°C)	Density, ρ (kg/m^3)	Specific Weight[b], γ (kN/m^3)	Dynamic Viscosity, μ (N·s/m^2)	Kinematic Viscosity, ν (m^2/s)	Surface Tension[c], σ (N/m)	Vapor Pressure, p_v [N/m^2(abs)]	Speed of Sound[d], c (m/s)
0	999.9	9.806	1.787 E − 3	1.787 E − 6	7.56 E − 2	6.105 E + 2	1403
5	1000.0	9.807	1.519 E − 3	1.519 E − 6	7.49 E − 2	8.722 E + 2	1427
10	999.7	9.804	1.307 E − 3	1.307 E − 6	7.42 E − 2	1.228 E + 3	1447
20	998.2	9.789	1.002 E − 3	1.004 E − 6	7.28 E − 2	2.338 E + 3	1481
30	995.7	9.765	7.975 E − 4	8.009 E − 7	7.12 E − 2	4.243 E + 3	1507
40	992.2	9.731	6.529 E − 4	6.580 E − 7	6.96 E − 2	7.376 E + 3	1526
50	988.1	9.690	5.468 E − 4	5.534 E − 7	6.79 E − 2	1.233 E + 4	1541
60	983.2	9.642	4.665 E − 4	4.745 E − 7	6.62 E − 2	1.992 E + 4	1552
70	977.8	9.589	4.042 E − 4	4.134 E − 7	6.44 E − 2	3.116 E + 4	1555
80	971.8	9.530	3.547 E − 4	3.650 E − 7	6.26 E − 2	4.734 E + 4	1555
90	965.3	9.467	3.147 E − 4	3.260 E − 7	6.08 E − 2	7.010 E + 4	1550
100	958.4	9.399	2.818 E − 4	2.940 E − 7	5.89 E − 2	1.013 E + 5	1543

Table 9 Different Types of river flows

$If\ R_e \leq 2000$	$If\ 2000 < R_e < 4000$	$If\ R_e > 4000$
Flow is Laminar	Flow is in transition zone	Flow is turbulent
Friction factor $f = \frac{64}{R_e}$	-	*Friction factor* $f = \left[1.8\log\left(\frac{R_e}{7}\right)\right]^{-2}$

4.14 Power Production

A generator is a crucial part of the hydropower plant. The generator primarily converts the shaft rotation into electric power [72]. The turbine and generator efficiencies are 89 % and 95 % respectively. The power acquired at the input of the turbine is determined by Equation 3-13 and it is found to be 590.57 kW, while the average power capability of the generator, which constitutes the output power, is derived from Equation 3-21 and it is 499.328 kW.

P = 1000 x 9.81 x 0.3 x 200.67 m = 590571.81 W = 590.57 kW

P_{av} = 9.81 x 200.67 x 0.3 x 0.89 x 0.95 = 499.328 kW

Friction losses for the maximum power production are one-third of the gross head and these losses are determined using Equation 3-20; these friction losses are then subtracted from the gross head to achieve the net head of the system as shown in Equation 3-14, assuming negligible local losses. Frictional losses and the system net head were computed to be 100.33 m and 200.67 m, respectively.

$$h_f = \frac{301}{3} =$$

100.33 m

h_n = 301 – 100.33 = 200.67 m

4.15 Total Stored Energy in the upper reservoir

The total energy stored in the upper reservoir was determined using Equation 3-22, resulting in a value of 24,544,815.15 kWh.

$$E = \frac{176{,}960{,}504 \; x \; 499.328 \; x \; 0.31}{(0.31 \; x \; 3600)} = 24{,}544{,}815.15 \text{ kWh}$$

4.16 Turbine selection

The Turbine Pro software was utilized to determine the output power that will be generated from the PHES. Figure 22 was utilised to determine the type of turbine to be used. Based on the design discharge, net head and potential power production, the Turgo turbine was selected. The Turgo turbine possesses an advantage over its counterpart turbines such as the Pelton turbine due to its unique runner design resembling a split Pelton runner. Consequently, for an equivalent power output, the diameter of the Turgo turbine's runner is halved compared to that of the Pelton turbine. This results in doubling the specific speed of the Turgo turbine [73]. At the maximum net head of 200 meters, the turbine can achieve a maximum output of 683 kW, while at the minimum head of 183.3 meters it can achieve a minimum power output of 598 kW as depicted in Figure 48.

Once the appropriate turbine has been chosen, the subsequent stage involves establishing the turbine's specific speed and determining the diameter of the turbine runner. The rotational speed was calculated using Equation 3-23 and was found as 1000 rpm while the specific speed was found through Equation 3-24 to be 10.29 rpm.

$$N = \frac{60x50}{0.5\ x\ 6} = 1000 \text{ rpm}$$

$$N_s = \frac{1000\ x\ \sqrt{0.3}}{200^{0.75}} = 10.29 \text{ rpm}$$

Runner diameter (D_{runner}) determines the turbine size and civil engineering cost hence it is important for selection of turbines. The runner diameter for the Turgo turbine to be used in the present study is determined using Equation 3-25 and was found to be 0.013 m.

$$D_{runner} = 84.5(0.79+1.602\ x\ 10.29)\frac{\sqrt{0.3}}{60\ x\ 1000} = 0.013 \text{ m}$$

Table 10 Turbines, specific speeds and Elevation head required

Type of Turbine	Aproximate Specific Speed	Head Required
Pelton Wheel	4	520
Turgot	7 to 15	335 to 180
Francis	15 to 100	180 to 40
Propeller	100 to 200	40 to 23

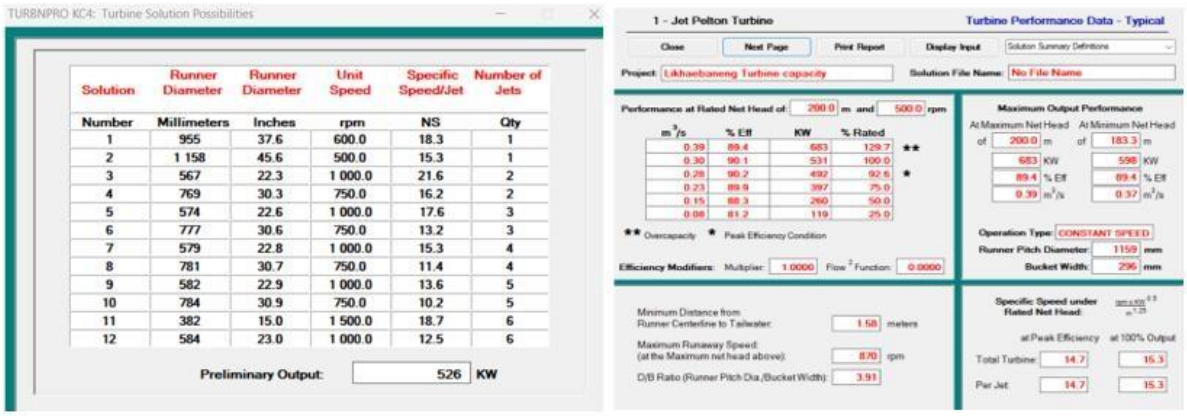

Figure 48 Turbine Pro software outputs

4.17 Cavitation

Equation 3-26 - Equation 3-30 were utilized to determine both the cross-sectional area of flow and the velocity at the valve outlet. In Equation 3-9, the diameter (d) of the penstock was found to be 0.529 m; therefore the radius (r) of the penstock is calculated in Equation 3-26 and it was found to be 0.2645 m.

$$r = \frac{0.529\ m}{2} = 0.2645 \text{ m}$$

Area of penstock at the upper reservoir (A_1) was calculated using Equation 3-27 and was found to be $0.2197\ m^2$

$$A_1 = 3.14 \times (0.2645)^2 = 0.2197\ m^2$$

velocity of water at the penstock inlet at the upper reservoir (V_1) was determined using Equation 3-28 and was found to be 1.37 m/s.

$$V_1 = \frac{0.3\ m^3/s}{0.2197\ m2} = 1.37\ m/s$$

Velocity of water at the exit valve was determine using Equation 3-29 to be 108.68 m/s.

$$V_2 = \sqrt{2261m \times 2 \times 9.81\ m/s^2 + (1.37\ m/s)^2 - 1960m \times 2 \times 9.81\ m/s^2 - (1960m - 2261m) \times 2 \times 9.81\ m/s^2} = 108.68\ m/s$$

Equation 3-30 was used to determine the cross-sectional area at the exit valve and was found to be 2.7604 x 10^{-3} m^2

$$A^2 = \frac{1080.3.68 m3\ m/s/s}{-3m2} = 2.7604 \times 10$$

5. Conclusion and recommendations

5.1 Conclusion

Utilizing photovoltaic and wind installations presents highly economical means of providing electricity to regions that would otherwise face lengthy wait periods for connection to the national power grid. The availability of resources for power generation was assessed, showing that water resources are low on average from May to September, with July having the lowest average rainfall at 15.17 mm. In contrast, the rest of the year receives sufficient rainfall, with January having the highest average at 130.82 mm. The average wind speed was found to be 4.85 m/s at 30 m a.g.l and solar resources were found to be adequate for power generation at 5.19 kWh/m^2/day. It was also found that, similar to water resources, solar resources are low from May to August. However, wind resources peak during this period, effectively compensating for the reduced water and solar supply.

HOMER software was employed to optimize the system, resulting in a selected configuration with a cost of energy of $0.2053 per kilowatt-hour (kWh) equivalent to M3.95 per kWh, and a maximum power production of 590.57 kW. This setup system has the NPC of $46.48 million and an initial investment of $29.29 million. Every year, the system produces 8,074,658 kWh through solar sources, making up 58.2 % of the total output. In addition, wind resources contribute 5,797,867 kWh annually, representing 41.8 % of the system's total energy production of 13,872,525 kWh. Consumption stands at 8,764,589 kWh per year, resulting in an energy surplus of 28.9 %. The system will be engineered to accommodate potential integration with the national grid if it reaches the area during the system's lifespan. This design will offer the flexibility to connect to the grid while also allowing operation during grid shutdowns or power cuts.

5.2 Recommendations

Pumped hydro energy storage (PHES) is the most efficient method of energy storage, especially for countries like Lesotho that have abundant water resources in their mountainous regions. Despite the abundance of water, the remote location of these areas makes it financially impractical to extend the national grid there in the near future, leaving most of Lesotho's population who live in these rural areas without access to electricity. Therefore, it is

recommended to conduct a comprehensive feasibility study on the construction of PHES systems, not only in the Quthing region but also throughout the country, particularly in rural areas. This will help achieve the goals of Lesotho's National Climate Change Policy which runs from 2017 to 2027 [74], by addressing the urgent issue of climate change and promoting the use of renewable energy sources.

The use of clean and sustainable resources such as water, solar, and wind for power generation is essential to combat climate change and provide electricity to underserved areas.
Comprehensive research into the availability of these resources across Lesotho is necessary to identify regions with adequate resources and initiate similar projects. This approach will help extend electricity access to rural areas, thereby boosting the economy and improving health outcomes.

The watershed area method used in this study to calculate the flow rate of the Likhaebaneng River is a theoretical approach for measuring flow rates of rivers without gauging stations. Thus, it is recommended that the flow rates of the involved rivers be measured physically to ensure accuracy.

References

[1] F. Scheifele, M. Bräuning, and B. Probst, "The impact of local content requirements on the development of export competitiveness in solar and wind technologies," *Renew. Sustain. Energy Rev.*, vol. 168, p. 112831, Oct. 2022, doi: 10.1016/j.rser.2022.112831.

[2] R. 2020 IEA, "Renewables 2020 - Analysis and forecast to 2025," 2020, [Online]. Available: https://iea.blob.core.windows.net/assets/1a24f1fe-c971-4c25-964a57d0f31eb97b/Renewables_2020

[3] "Renewables 2022 Global Status Report United States of America Factsheet | Policy Commons." Accessed: Oct. 08, 2023. [Online]. Available: https://policycommons.net/artifacts/2471826/renewables-2022-global-status-reportunited-states-of-america-factsheet/3493831/

[4] "Lesotho Submits its Climate Action Plan Ahead of 2015 Paris Agreement | UNFCCC." Accessed: Oct. 08, 2023. [Online]. Available: https://unfccc.int/news/lesotho-submits-itsclimate-action-plan-ahead-of-2015-paris-agreement

[5] L. Qiu, L. He, H. Lu, and D. Liang, “Pumped hydropower storage potential and its contribution to hybrid renewable energy co-development: A case study in the QinghaiTibet Plateau,” *J. Energy Storage*, vol. 51, p. 104447, Jul. 2022, doi: 10.1016/j.est.2022.104447.

[6] S. H. Sterl, *Sterl - 2021 - Seasons of Power - Streamlining strategies for renewable electricity generation from sun, wind and water in sub-Saharan Africa.pdf*. Vrije Universiteit Brussel.

[7] M. D’Isidoro *et al.*, “Estimation of solar and wind energy resources over Lesotho and their complementarity by means of WRF yearly simulation at high resolution,” *Renew. Energy*, vol. 158, pp. 114–129, Oct. 2020, doi: 10.1016/j.renene.2020.05.106.

[8] S. Tsoeu-Ntokoane, M. Kali, and X. Lemaire, “Energy democracy in Lesotho: Prioritising the participation of rural citizens,” *Cogent Soc. Sci.*, p. 17, 2022.

[9] B. M. Taele, L. Mokhutšoane, and I. Hapazari, “An overview of small hydropower development in Lesotho: Challenges and prospects,” *Renew. Energy*, vol. 44, pp. 448–452, Aug. 2012, doi: 10.1016/j.renene.2012.01.086.

[10] M. Petrollese, P. Seche, and D. Cocco, “Analysis and optimization of solar-pumped hydro storage systems integrated in water supply networks,” *Energy*, vol. 189, p. 116176, Dec. 2019, doi: 10.1016/j.energy.2019.116176.

[11] L. Ruppert, R. Schürhuber, B. List, A. Lechner, and C. Bauer, “An analysis of different pumped storage schemes from a technological and economic perspective,” *Energy*, vol. 141, pp. 368–379, Dec. 2017, doi: 10.1016/j.energy.2017.09.057.

[12] X. Wen *et al.*, “Optimizing the sizes of wind and photovoltaic plants complementarily operating with cascade hydropower stations: Balancing risk and benefit,” *Appl. Energy*, vol. 306, p. 117968, Jan. 2022, doi: 10.1016/j.apenergy.2021.117968.

[13] T. Ma, H. Yang, L. Lu, and J. Peng, “Technical feasibility study on a standalone hybrid solar-wind system with pumped hydro storage for a remote island in Hong Kong,” *Renew. Energy*, vol. 69, pp. 7–15, Sep. 2014, doi: 10.1016/j.renene.2014.03.028.

[14] J. Zhang, C. Cheng, S. Yu, J. Shen, X. Wu, and H. Su, “Preliminary feasibility analysis for remaking the function of cascade hydropower stations to enhance hydropower flexibility: A case study in China,” *Energy*, vol. 260, p. 125163, Dec. 2022, doi: 10.1016/j.energy.2022.125163.

[15] K. Huang, P. Liu, B. Ming, J.-S. Kim, and Y. Gong, “Economic operation of a wind-solarhydro complementary system considering risks of output shortage, power curtailment and spilled water,” *Appl. Energy*, vol. 290, p. 116805, May 2021, doi: 10.1016/j.apenergy.2021.116805.

[16] L. Lu *et al.*, “Optimization model for the short-term joint operation of a grid-connected wind-photovoltaic-hydro hybrid energy system with cascade hydropower plants,” *Energy Convers. Manag.*, vol. 236, p. 114055, May 2021, doi: 10.1016/j.enconman.2021.114055.

[17] T. Ma, H. Yang, L. Lu, and J. Peng, “Pumped storage-based standalone photovoltaic power generation system: Modeling and techno-economic optimization,” *Appl. Energy*, vol. 137, pp. 649–659, Jan. 2015, doi: 10.1016/j.apenergy.2014.06.005.

[18] M. Senatla, M. Nchake, B. M. Taele, and I. Hapazari, “Electricity capacity expansion plan for Lesotho – implications on energy policy,” *Energy Policy*, vol. 120, pp. 622–634, Sep. 2018, doi: 10.1016/j.enpol.2018.06.003.

[19] M. Zeidan, M. Al-soud, M. Dmour, Z. Alakayleh, and S. Al-qawabah, “Integrating a Solar PV System with Pumped Hydroelectric Storage at the Mutah University of Jordan,” *Energies*, vol. 16, no. 15, p. 5769, Aug. 2023, doi: 10.3390/en16155769.

[20] “Grid stability in the MENA countries: Can pumped... - Google Scholar.” Accessed: Oct. 11, 2023. [Online]. Available: https://scholar.google.com/scholar?hl=en&as_sdt=0%2C5&q=Grid+stability+in+the+MENA+countries%3A+Can+pumped+storage+support+grid+integration+of+renewables&btnG=

[21] P. H. Gleick, “Climate change, hydrology, and water resources,” *Rev. Geophys.*, vol. 27, no. 3, pp. 329–344, 1989, doi: 10.1029/RG027i003p00329.

[22] O. US EPA, “Climate Change Indicators: Atmospheric Concentrations of Greenhouse Gases.” Accessed: Jul. 30, 2024. [Online]. Available: https://www.epa.gov/climateindicators/climate-change-indicators-atmospheric-concentrations-greenhouse-gases

[23] L. Lekhanya, “analysis-of-quthing-river-and-letseng-la-letsie-for-hydropowerpotential.pdf,” *Lesotho Natl. Univ. Lesotho*, 2020, [Online]. Available: https://repository.tml.nul.ls/

[24] L. Lekhanya, “analysis-of-quthing-river-and-letseng-la-letsie-for-hydropowerpotential.pdf,” National University of Lesotho, Roma, Lesotho, 2020.

[25] C. C. Gianfagna, C. E. Johnson, D. G. Chandler, and C. Hofmann, “Watershed area ratio accurately predicts daily streamflow in nested catchments in the Catskills, New York,” *J. Hydrol. Reg. Stud.*, vol. 4, pp. 583–594, Sep. 2015, doi: 10.1016/j.ejrh.2015.09.002.

[26] E. J. Kennedy, “Discharge Ratings at Gaging Stations; Department of the Interior,” *US Geol. Surv.*, 1984.

[27] M. Mpholo, T. Mathaba, and M. Letuma, “Wind profile assessment at Masitise and Sani in Lesotho for potential off-grid electricity generation,” *Energy Convers. Manag.*, vol. 53, no. 1, pp. 118–127, Jan. 2012, doi: 10.1016/j.enconman.2011.07.015.

[28] M. Nedaei, E. Assareh, and M. Biglari, “An extensive evaluation of wind resource using new methods and strategies for development and utilizing wind power in Mah-shahr station in Iran,” *Energy Convers. Manag.*, vol. 81, pp. 475–503, May 2014, doi: 10.1016/j.enconman.2014.02.025.

[29] J. Wang, S. Qin, S. Jin, and J. Wu, “Estimation methods review and analysis of offshore extreme wind speeds and wind energy resources,” *Renew. Sustain. Energy Rev.*, vol. 42, pp. 26–42, Feb. 2015, doi: 10.1016/j.rser.2014.09.042.

[30] P. Wais, “A review of Weibull functions in wind sector,” *Renew. Sustain. Energy Rev.*, vol. 70, pp. 1099–1107, Apr. 2017, doi: 10.1016/j.rser.2016.12.014.

[31] M. Sathyajith, “Wind energy: fundamentals, resource analysis and economics,” *Choice Rev. Online*, vol. 44, no. 01, pp. 44-0337-44–0337, Sep. 2006, doi: 10.5860/CHOICE.440337.

[32] A. Blakers, M. Stocks, B. Lu, C. Cheng, and R. Stocks, “Pathway to 100% Renewable Electricity,” *IEEE J. Photovolt.*, vol. 9, no. 6, pp. 1828–1833, Nov. 2019, doi: 10.1109/JPHOTOV.2019.2938882.

[33] “Wind energy: fundamentals, resource analysis and economics,” *Choice Rev. Online*, vol. 44, no. 01, pp. 44-0337-44–0337, Sep. 2006, doi: 10.5860/CHOICE.44-0337.

[34] S. Mathew, *Wind Energy*. Berlin, Heidelberg: Springer Berlin Heidelberg, 2006. doi: 10.1007/3-540-30906-3.

[35] D. H. Muhsen, T. Khatib, and F. Nagi, "A review of photovoltaic water pumping system designing methods, control strategies and field performance," *Renew. Sustain. Energy Rev.*, vol. 68, pp. 70–86, Feb. 2017, doi: 10.1016/j.rser.2016.09.129.

[36] G. K. Singh, "Solar power generation by PV (photovoltaic) technology: A review," *Energy*, vol. 53, pp. 1–13, May 2013, doi: 10.1016/j.energy.2013.02.057.

[37] A.-K. Daud and M. M. Mahmoud, "Solar powered induction motor-driven water pump operating on a desert well, simulation and field tests," *Renew. Energy*, vol. 30, no. 5, pp. 701–714, Apr. 2005, doi: 10.1016/j.renene.2004.02.016.

[38] J. S. Ramos and H. M. Ramos, "Solar powered pumps to supply water for rural or isolated zones: A case study," *Energy Sustain. Dev.*, vol. 13, no. 3, pp. 151–158, Sep. 2009, doi: 10.1016/j.esd.2009.06.006.

[39] K. E. Sarah and U. Roland, "A Review of Solar Photovoltaic Technologies," *Int. J. Eng. Res.*, vol. 9, no. 07.

[40] B. Parida, S. Iniyan, and R. Goic, "A review of solar photovoltaic technologies," *Renew. Sustain. Energy Rev.*, vol. 15, no. 3, pp. 1625–1636, Apr. 2011, doi: 10.1016/j.rser.2010.11.032.

[41] K. E. Sarah and U. Roland, "A Review of Solar Photovoltaic Technologies," *Int. J. Eng. Res.*, vol. 9, no. 07.

[42] "Types Of Solar Panels: Which One Is The Best Choice?" Accessed: Jul. 28, 2024. [Online]. Available: https://www.solarreviews.com/blog/pros-and-cons-ofmonocrystalline-vs-polycrystalline-solar-panels

[43] M. Powalla *et al.*, "Advances in Cost-Efficient Thin-Film Photovoltaics Based on Cu(In,Ga)Se2," *Engineering*, vol. 3, no. 4, pp. 445–451, Aug. 2017, doi: 10.1016/J.ENG.2017.04.015.

[44] C.-J. Yang, "Transparent conducting aluminium doped zinc oxide for silicon quantum dot solar cell devices in third generation photovoltaics," UNSW Sydney, 2015. doi: 10.26190/UNSWORKS/18815.

[45] B. M. Başol and B. McCandless, "Brief review of cadmium telluride-based photovoltaic technologies," *J. Photonics Energy*, vol. 4, no. 1, p. 040996, Jun. 2014, doi: 10.1117/1.JPE.4.040996.

[46] S. Ouedraogo *et al.*, "Optimization of Copper Indium Gallium Di-Selenide (CIGS) based solar cells by back grading," in *2013 Africon*, Pointe-Aux-Piments, Mauritius: IEEE, Sep. 2013, pp. 1–6. doi: 10.1109/AFRCON.2013.6757813.

[47] S. Sagadevan, "RECENT TRENDS ON NANOSTRUCTURES BASED SOLAR ENERGY APPLICATIONS: A REVIEW".

[48] M. Bilgili, H. Bilirgen, A. Ozbek, F. Ekinci, and T. Demirdelen, "The role of hydropower installations for sustainable energy development in Turkey and the world," *Renew. Energy*, vol. 126, pp. 755–764, Oct. 2018, doi: 10.1016/j.renene.2018.03.089.

[49] A. Blakers, M. Stocks, B. Lu, and C. Cheng, "A review of pumped hydro energy storage," *Prog. Energy*, vol. 3, no. 2, p. 022003, Apr. 2021, doi: 10.1088/2516-1083/abeb5b.

[50] F. A. Canales and A. Beluco, “Modeling pumped hydro storage with the micropower optimization model (HOMER),” *J. Renew. Sustain. Energy*, vol. 6, no. 4, p. 043131, Jul. 2014, doi: 10.1063/1.4893077.

[51] S. M. Islam, “Increasing wind energy penetration level using pumped hydro storage in island micro-grid system,” 2012.

[52] F. A. Canales and A. Beluco, “Modeling pumped hydro storage with the micropower optimization model (HOMER),” *J. Renew. Sustain. Energy*, vol. 6, no. 4, p. 043131, Jul. 2014, doi: 10.1063/1.4893077.

[53] M. Mahmouda, M. Ramadanc, A.-G. Olabie, K. Pullena, and S. Nahera, “A review of mechanical energy storage systems combined with wind and solar.pdf,” *Elsevier*, 2020, [Online]. Available: www.elsevier.com/locate/enconman

[54] E. N. Nyeche and E. O. Diemuodeke, “Modelling and optimisation of a hybrid PV-wind turbine-pumped hydro storage energy system for mini-grid application in coastline communities,” *J. Clean. Prod.*, vol. 250, p. 119578, Mar. 2020, doi: 10.1016/j.jclepro.2019.119578.

[55] A. Morabito, J. Steimes, O. Bontems, G. Al Zohbi, and P. Hendrick, “Set-up of a pump as turbine use in micro-pumped hydro energy storage: a case of study in Froyennes Belgium,” *J. Phys. Conf. Ser.*, vol. 813, p. 012033, Apr. 2017, doi: 10.1088/17426596/813/1/012033.

[56] “Cost and revenue breakdown for a pumped hydroelectric... - Google Scholar.” Accessed: Oct. 18, 2023. [Online]. Available: https://scholar.google.com/scholar?hl=en&as_sdt=0%2C5&q=Cost+and+revenue+breakdown+for+a+pumped+hydroelectric+energy+storage+installation+in+Belgium&btnG=

[57] O. Paish, “Micro-hydropower: Status and prospects,” *Proc. Inst. Mech. Eng. Part J. Power Energy*, vol. 216, no. 1, pp. 31–40, Feb. 2002, doi: 10.1243/095765002760024827.

[58] T. Syverud and R. Ascoli, “Technical characteristics of a hydropower plant.,” *Aquila Cap.*, 2019, [Online]. Available: www.aquila-capital.de

[59] D. Bashir, “HYDROLOGICAL STUDIES FOR SMALL HYDROPOWER PLANNING.pdf,” *Anam.-Imo River Basin Dev. Auth. Owerri 26-30 May 2003*, 2003, [Online]. Available: https://d1wqtxts1xzle7.cloudfront.net/35712197

[60] D. S., M. Chadaga, U. Lathashri, S. Salim, A. Jyoti, and S. Pant, “Assessment of Streamflow Characteristics in a Watershed Using Flow Duration Curves and Hydrograph Analysis:,” in *Proceedings of the 3rd International Symposium on Water, Ecology and Environment*, Beijing, China: SCITEPRESS - Science and Technology Publications, 2022, pp. 90–95. doi: 10.5220/0011907500003536.

[61] V. Costa, W. Fernandes, and Â. Starick, “Identifying Regional Models for Flow Duration Curves with Evolutionary Polynomial Regression: Application for Intermittent Streams,” *J. Hydrol. Eng.*, vol. 25, no. 1, p. 04019059, Jan. 2020, doi: 10.1061/(ASCE)HE.19435584.0001873.

[62] “Water Resources Systems Planning and Management:... - Google Scholar.” Accessed: Jul. 11, 2024. [Online]. Available: https://scholar.google.com/scholar?hl=en&as_sdt=0%2C5&q=Water+Resources+Syste

ms+Planning+and+Management%3A+An+Introduction+to+Methods%2C+Models+and+Applications&btnG=

[63] Q. Tan, Z. Nie, X. Wen, H. Su, G. Fang, and Z. Zhang, "Complementary scheduling rules for hybrid pumped storage hydropower-photovoltaic power system reconstructing from conventional cascade hydropower stations - ScienceDirect," vol. 288, Jul. 2024, doi: 10.1016.

[64] H. Li, P. Liu, S. Guo, B. Ming, L. Cheng, and Z. Yang, "Long-term complementary operation of a large-scale hydro-photovoltaic hybrid power plant using explicit stochastic optimization," *Appl. Energy*, vol. 238, pp. 863–875, Mar. 2019, doi: 10.1016/j.apenergy.2019.01.111.

[65] M. S. Javed, T. Ma, J. Jurasz, and M. Y. Amin, "Solar and wind power generation systems with pumped hydro storage: Review and future perspectives," *Renew. Energy*, vol. 148, pp. 176–192, Apr. 2020, doi: 10.1016/j.renene.2019.11.157.

[66] "HOMER Pro - Microgrid Software for Designing Optimized Hybrid Microgrids." Accessed: Nov. 20, 2023. [Online]. Available: https://www.homerenergy.com/products/pro/index.html

[67] "Optimization and designing of hybrid power system using HOMER pro," *Mater. Today Proc.*, vol. 47, pp. S110–S115, Jan. 2021, doi: 10.1016/j.matpr.2020.06.054.

[68] H. Shahinzadeh, G. B. Gharehpetian, S. H. Fathi, and S. M. Nasr-Azadani, "Optimal Planning of an Off-grid Electricity Generation with Renewable Energy Resources using the HOMER Software," *Int. J. Power Electron. Drive Syst. IJPEDS*, vol. 6, no. 1, p. 137, Mar. 2015, doi: 10.11591/ijpeds.v6.i1.pp137-147.

[69] S. W. Grab and D. J. Nash, "Documentary evidence of climate variability during cold seasons in Lesotho, southern Africa, 1833–1900," *Clim. Dyn.*, vol. 34, no. 4, pp. 473–499, Mar. 2010, doi: 10.1007/s00382-009-0598-4.

[70] "Canales and Beluco - 2014 - Modeling pumped hydro storage with the micropower .pdf."

[71] M. Mpholo, D. Steuerwald, and T. Kukeera, Eds., *Africa-EU Renewable Energy Research and Innovation Symposium 2018 (RERIS 2018): 23–26 January 2018, National University of Lesotho On occasion of NULISTICE 2018*. in Springer Proceedings in Energy. Cham: Springer International Publishing, 2018. doi: 10.1007/978-3-319-93438-9.

[72] C. P. Jawahar and P. A. Michael, "A review on turbines for micro hydro power plant," *Renew. Sustain. Energy Rev.*, vol. 72, pp. 882–887, May 2017, doi: 10.1016/j.rser.2017.01.133.

[73] L. Team, "What is Turgo Turbine and How does it Work? | Linquip." Accessed: Apr. 11, 2024. [Online]. Available: https://www.linquip.com/blog/turgo-turbine/

[74] M. D'Isidoro *et al.*, "Estimation of solar and wind energy resources over Lesotho and their complementarity by means of WRF yearly simulation at high resolution," *Renew. Energy*, vol. 158, pp. 114–129, Oct. 2020, doi: 10.1016/j.renene.2020.05.106.